ACS MATERIALS LETTERS

www.acsmaterialsletters.org

LETTER

Rational Construction of Ultrahigh Thermal Stable MOF for Efficient Separation of MTO Products and Natural Gas

Gang-Ding Wang, Rajamani Krishna, Yong-Zhi Li, Yao-Yu Ma, Lei Hou,* Yao-Yu Wang, and Zhonghua Zhu

Cite This: *ACS Materials Lett.* 2023, 5, 1091−1099

Read Online

ACCESS | Metrics & More | Article Recommendations | Supporting Information

ABSTRACT: **Considering the important application foundation of propylene (C_3H_6) and ethylene (C_2H_4) production, as well as methane (CH_4), in petrochemical industries, this report comprehensively investigated an innovative MOF material (Zn-BPZ-SA) that was synthesized by 3,3′,5,5′-tetramethyl-4,4′-bipyrazole (H_2BPZ) and squaric acid (H_2SA) for separating methanol-to-olefins (MTO) products (C_3H_6/C_2H_4 mixtures) and natural gas ($C_3H_8/C_2H_6/CH_4$ mixtures). Zn-BPZ-SA with great resistance toward water and exceptional thermal stability (520 °C), can preferentially adsorb C_3H_8 and C_3H_6 rather than C_2H_6 and C_2H_4, and in particular, reveals high C_3H_6 and C_3H_8 uptakes of 46.6 and 48.0 $cm^3\ g^{-1}$ under the crucial low pressure (10 kPa, 298 K). The experimental and simulated transient breakthroughs for C_3H_6/C_2H_4 binary mixtures and $C_3H_8/C_2H_6/CH_4$ ternary mixtures demonstrated that the MOF can separate these mixtures with long breakthrough time differences, yielding high-purity (>99.95%) products with high productivities: C_2H_4 (21.9−142.8 L kg^{-1}) and CH_4 (34.9−73.0 L kg^{-1}). The excellent separation abilities can be attributed to the rich accessbile O/N and methyl binding sites scattered at the pore surfaces in framework.**

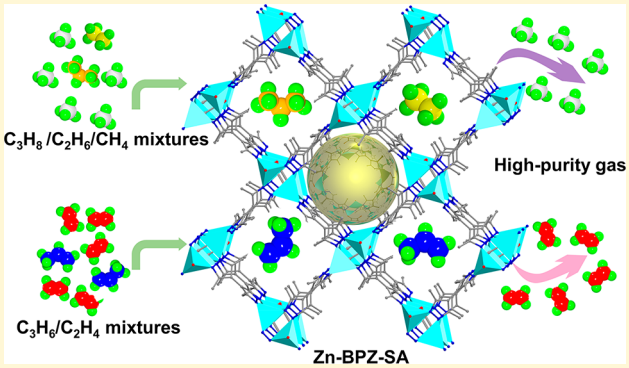

Propylene (C_3H_6) and ethylene (C_2H_4) are crucial energy resources and also vitally important feedstocks in the chemical process industry.[1−3] The total global production of C_2H_4 and C_3H_6 ranks as the most chemical raw materials in the world.[4,5] The methanol-to-olefins (MTO) reaction is an important and advanced method for preparing C_2H_4 from coal and natural gas, where the products contain ∼21 wt % C_3H_6 and ∼51 wt % C_2H_4.[6,7] Therefore, separating C_3H_6 and C_2H_4 of MTO products is essential for downstream applications. The common separation process of C_3H_6 and C_2H_4 mixtures is mainly dependent upon the cryogenic distillation at high pressure, requiring large energy consumption accounting for more than 0.3% of the global energy needs.[8−10] Besides olefins, a second critical separation object is natural gas, predominantly composed of methane (CH_4, 85%), ethane (C_2H_6, 9%), and propane (C_3H_8, 3%).[11] Natural gas is considered as an important clean energy due to the main component of CH_4 with high hydrogen-to-carbon ratio and low carbon dioxide emissions.[12] However, the coexisting C_2H_6 and C_3H_8 not only reduces the efficiency of CH_4 combustion but also raises the risk of equipment fouling and pipeline clogging.[13−15] So C_2H_6 and C_3H_8 impurities have to be removed from CH_4 prior to transportation process, through the highly energy-intensive cryogenic distillation technology in industry. It is widely believed that transition to adsorbent-based separation strategy with much low energy consumption and safe operation would be of great importance for gas purification.[16−19] Consequently, there is an urgent demand to develop adsorbents for hydrocarbon separation goal under mild conditions.

Metal−organic frameworks (MOFs) with the variety of topologies meet the task-specific application requirements.[20−27] The prominent advantages of MOFs over the zeolites and carbon adsorbents are their precisely controllable pores and easy modifications, which display unparalleled performance for gases

Received: January 30, 2023
Accepted: March 7, 2023

https://doi.org/10.1021/acsmaterialslett.3c00096
ACS Materials Lett. 2023, 5, 1091−1099

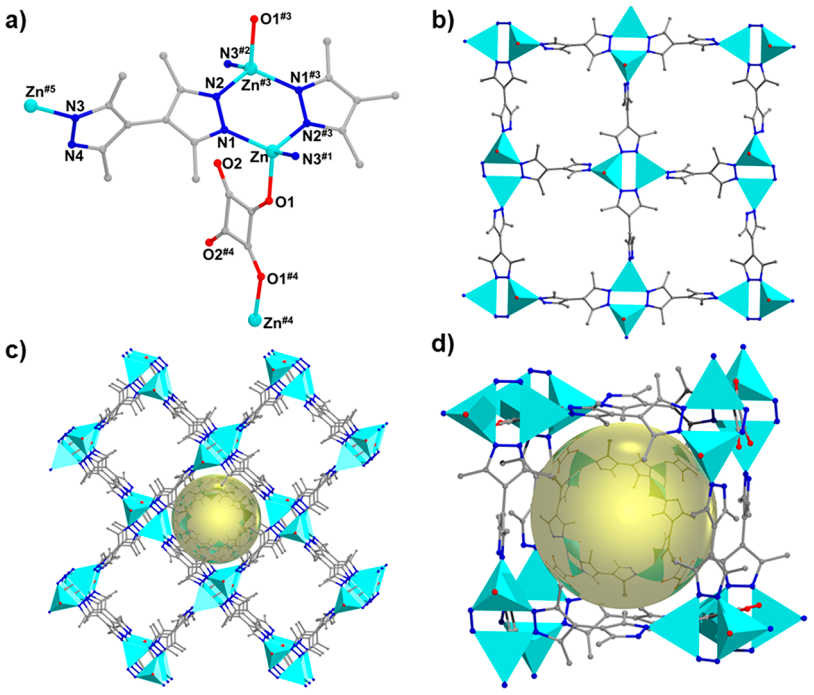

Figure 1. (a) Coordination environment of Zn^{2+} ions, (b) 2D layer, (c) 3D framework viewed along the *c* axis, and (d) cage in Zn-BPZ-SA (N, blue; O, red; C, gray; Zn, turquoise).

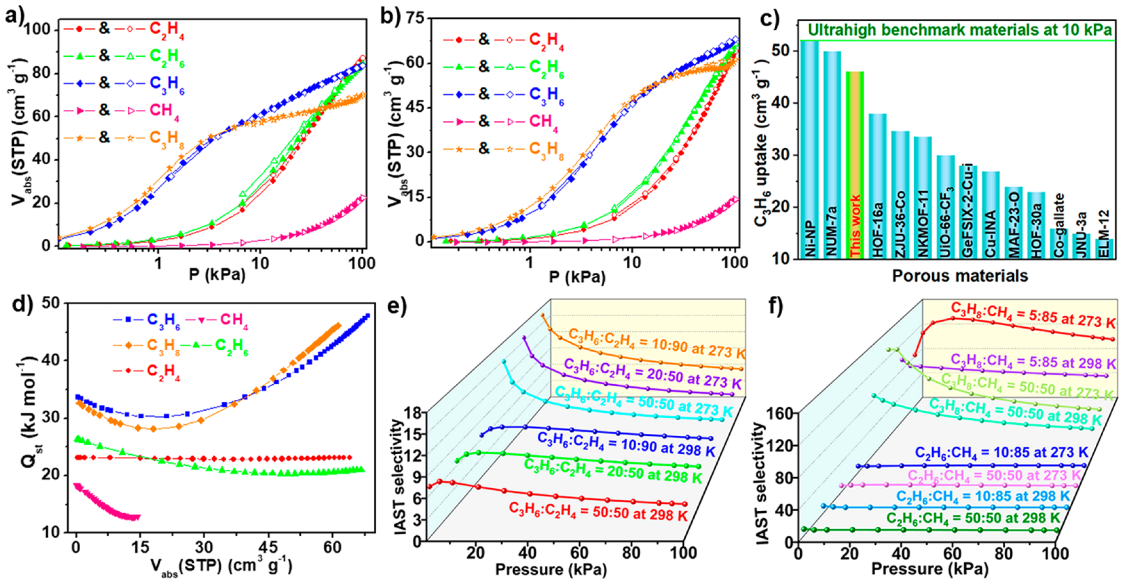

Figure 2. Gas sorption isotherms of Zn-BPZ-SA at (a) 273 K and (b) 298 K. (c) Comparisons of C_3H_6 uptakes in different porous materials at 298 K under 10 kPa; (d) Q_{st} of Zn-BPZ-SA for different gases; and IAST selectivities of Zn-BPZ-SA for (e) C_3H_6/C_2H_4 and (f) C_2H_6/CH_4 and C_3H_8/CH_4.

and obtain remarkable progress in gas separation application, including Xe/Kr, C_2H_6/C_2H_4, C_2H_2/CO_2, C_3H_6/C_3H_8, and so on.[28−35] However, the less commonly reported MOFs displayed the separation for C_3/C_2 hydrocarbons, especially for C_3H_6/C_2H_4.[7,36] In addition, water vapor often coexists with the feed gases in separation process, which will greatly degrade the separation performance of adsorbents, thus the stability of MOFs is a prerequisite for utilization from an industrial point of view. Many efforts have been devoted improving the thermal and chemical stability of MOFs, including adopting high-oxidation-state metal ions or clusters.[37] On the other hand, from the aspect of organic building units, using pyrazole linkers with high pK_a and introducing hydrophobic organic groups are also effective to form porous networks with great stability.[38]

For separation goal of MTO products and natural gas, a new pillared-layer MOF, $[Zn(HBPZ)(SA)_{0.5}]\cdot 3H_2O\cdot 0.25DMF$ (Zn-BPZ-SA) was herein created by employing 3,3′,5,5′-tetramethyl-4,4′-bipyrazole (H_2BPZ) and squaric acid (H_2SA) linkers. The utilization of pyrazole coordinated units and the incoporation of methyl groups in ligands endow Zn-BPZ-SA with great resistance toward water and exceptional thermal stability beyond 500 °C. The static gas adsorptions and experimental breakthroughs indicate that Zn-BPZ-SA can preferentially adsorb and separate C_3H_6 from C_3H_6/C_2H_4 mixtures, as well

https://doi.org/10.1021/acsmaterialslett.3c00096
ACS Materials Lett. 2023, 5, 1091−1099

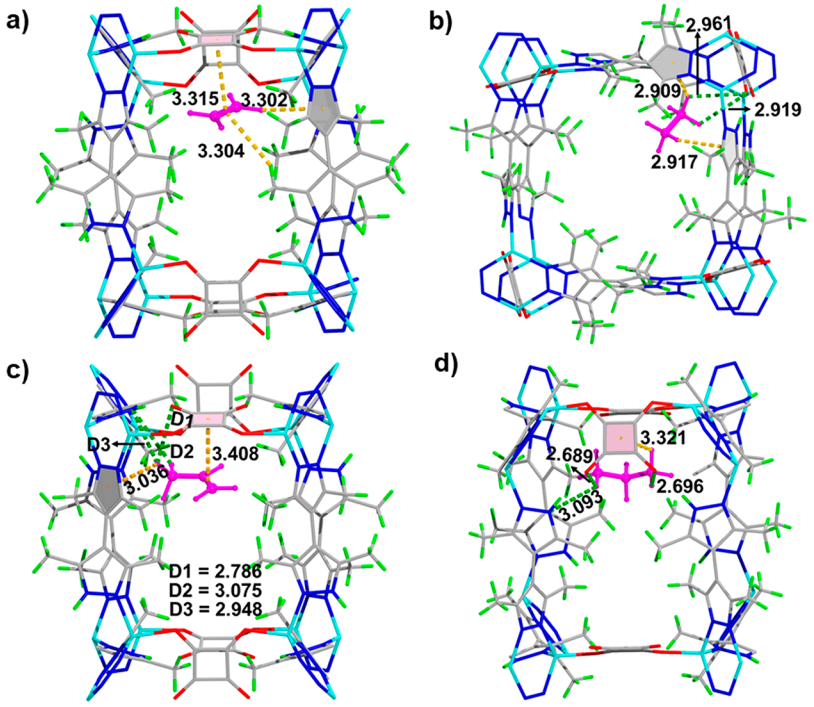

Figure 3. Preferential binding sites for (a) C_2H_4; (b) C_2H_6; (c) C_3H_6; and (d) C_3H_8 (N, blue; O, red; C, gray; Zn, turquoise; H, green).

as C_2H_6 and C_3H_8 from $C_3H_8/C_2H_6/CH_4$ mixtures, respectively. Grand Canonical Monte Carlo (GCMC) simulations revealed that the accessbile O/N and methyl binding sites are responsible for separation.

Zn-BPZ-SA crystallizes in tetragonal I_4/m space group and contains one Zn^{2+} ion, one HBPZ ligand, and a half of SA linker in the asymmetric unit. The Zn^{2+} ion has a N_3O tetrahedral coordinated geometry surrounded by three HBPZ ligands and one SA ligand (Figure 1a). Two pyrazolyl (pz) rings in two HPBZ bridge two Zn^{2+} ions to form a $[Zn_2(pz)_2]$ dimer. Adjacent dimers are interconnected by HBPZ to form grid layers (Figure 1b), and which are further jointed by SA pillars to produce a three-dimensional (3D) open layer-pillared framework (Figures 1c and S2). The framework contains cubelike cages composed of eight $[Zn_2(pz)_2]$ dimers, eight HBPZ, and four SA with the dimensions of $9.0 \times 10.7 \times 10.7$ Å^3 (Figure 1d), which was determined by measuring the distances between the centers of dimers. Two pyrazolyls of HBPZ are tilted with an angle of 69.8°, leading to all methyl groups of HBPZ direct inward in cages, giving rise to a reduced window size. The linkage among the cages produces a 3D intersected pore with the accessible void of 45.6% calculated by the 1.2 Å probe based on the PLATON program (Figure S3). The pore wall is mainly decorated by methyl groups, and uncoordinated O and N atoms from ligands, which would play a decisive role in gas adsorption and separation process.

The purity of bulk Zn-BPZ-SA was confirmed by measuring powder X-ray diffraction (PXRD) pattern that matches well with the simulated from crystal structure (Figure S4). At 77 K, N_2 sorption experiment of the desolvated Zn-BPZ-SA that was prepared by activation at 393 K exhibited reversible a type-I sorption isotherm (Figure S5), and the Langmuir and Brunauer–Emmett–Teller (BET) surface areas were 1013 and 925 $m^2\ g^{-1}$, respectively (Figure S6). The pore volume of 0.46 $cm^3\ g^{-1}$ is consistent with the value (0.47 $cm^3\ g^{-1}$) calculated from crystal structure. The pore size distribution localizes in 6.4–8.4 Å range based on density functional theory method (Figure S5).

Due to the existence of rich methyl groups and accessible O/N atoms in the pore wall of Zn-BPZ-SA, the sorption isotherms at 273 and 298 K for C_2H_4, C_2H_6, C_3H_6, C_3H_8, and CH_4 were measured to estimate separation performance. The adsorption curves of C_3H_6 and C_3H_8 exhibit steep rise at low pressure of 1–10 kPa, affording the ultrahigh C_3H_6 and C_3H_8 uptakes of 46.6/48.0 $cm^3\ g^{-1}$ at 298 K under 10 kPa (Figure 2a and 2b). This means that the interaction strengths of the framework to gases deferred to the order of $C_3 > C_2 > CH_4$, which is a crucial prerequisite for separating C_3H_6/C_2H_4 and $C_3H_8/C_2H_6/CH_4$. Zn-BPZ-SA maintains the high C_3H_6 uptake (46.6 $cm^3\ g^{-1}$) at 298 K under 10 kPa, surpassing the most reported outstanding materials, such as HOF-16a (38 $cm^3\ g^{-1}$),[39] ZU-36-Co (34.7 $cm^3\ g^{-1}$),[40] NKMOF-11 (33 $cm^3\ g^{-1}$),[41] and UiO-66-CF_3 (38 $cm^3\ g^{-1}$),[5] but slightly lower than some top-performance MOFs such as NUM-7a (50 $cm^3\ g^{-1}$)[42] and Ni-NP (52 $cm^3\ g^{-1}$)[43] (Figure 2c). At 298 and 273 K under 100 kPa, the loadings in Zn-BPZ-SA reach 63.9/87.2 $cm^3\ g^{-1}$ for C_2H_4, 66.6/84.6 $cm^3\ g^{-1}$ for C_2H_6, 68.3/83.8 $cm^3\ g^{-1}$ for C_3H_6, 61.2/70.5 $cm^3\ g^{-1}$ for C_3H_8, and 14.4/22.6 $cm^3\ g^{-1}$ for CH_4, respectively. The relative low loadings for C_3 hydrocarbons compared to C_2 hydrocarbons are not uncommon considering the larger bulks of C_3 molecules. Isosteric enthalpies of adsorption (Q_{st}) were calculated using the virial equation based on the adsorption data at 273 and 298 K to evaluate the affinity of Zn-BPZ-SA for gases (Figure S7–S11). As shown in Figure 2d, the Q_{st} values followed the hierarchy of $C_3 > C_2 > CH_4$, conferring the potential of separating $C_1/C_2/C_3$ alkanes and C_2/C_3 alkenes. The Q_{st} values gradually increase for C_3H_6 and C_3H_8 at higher coverage, differing from the cases of C_2H_6, C_2H_6, and CH_4, implying the C_3 adsorption benefits from the intermolecular interactions among the adsorbates.[44–46] Further, continuous C_2H_4 adsorption/desorption tests confirm easy recyclability of Zn-BPZ-SA with no capacity loss (Figure S12).

https://doi.org/10.1021/acsmaterialslett.3c00096
ACS Materials Lett. 2023, 5, 1091–1099

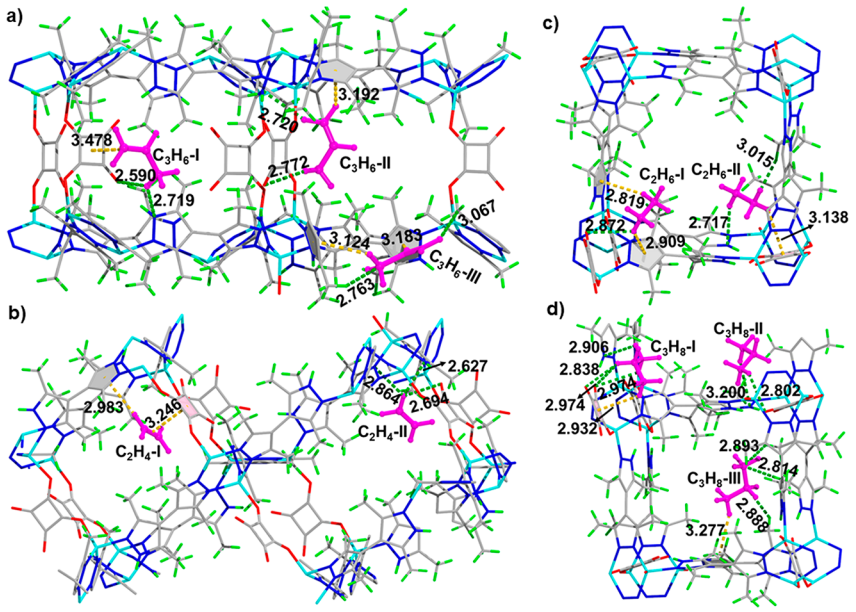

Figure 4. Adsorption sites for (a) C_3H_6; (b) C_2H_4; (c) C_2H_6; and (d) C_3H_8 in Zn-BPZ-SA simulated at 298 K under 100 kPa (N, blue; O, red; C, gray; Zn, turquiose; H, green).

The selectivities of Zn-BPZ-SA for C_3H_6/C_2H_4, C_2H_6/CH_4, and C_3H_8/CH_4 mixtures at 273 and 298 K were calculated by ideal adsorbed solution theory (IAST) on the basis of adsorption isotherms (Figure S13−S17, Tables S3 and S4). As illustrated in Figure 2e, the predicted C_3H_6/C_2H_4 selectivities for the 50/50, 20/50, and 10/90 C_3H_6/C_2H_4 mixtures are 4.8/5.3, 5.3/5.8, and 6.1/6.8 at 298/273 K under 100 kPa, respectively, which are considerably high in MOFs and are comparable to the reported excellent MOFs, such as $\{[Co_4(TC_4A)Cl](L)_2][(CH_3CH_2)_4N]\}_n$ (50/50 C_3H_6/C_2H_4 mixtures: 3.6 at 298 K and 4.6 at 273 K),[47] Ni-MOF-74 (50/50 C_3H_6/C_2H_4 mixtures: 3.3 at 298 K),[48] NEM-7-Cu (50/50 C_3H_6/C_2H_4 mixtures: 8.6 at 298 K; 10/90 C_3H_6/C_2H_4 mixtures: 8.5 at 298 K),[10] and UPC-33 (50/50 C_3H_6/C_2H_4 mixtures: 5.7 at 298 K; 10/90 C_3H_6/C_2H_4 mixtures: 5.84 at 298 K).[49] The selectivities of Zn-BPZ-SA for C_3H_8/CH_4 and C_2H_6/CH_4 mixtures that are related to the natural gas purification demand in industry were also calculated. Under 100 kPa, the IAST selectivities for various ratios of C_2H_6/CH_4 (50/50 and 10/85) and C_3H_8/CH_4 (50/50 and 5/85) mixtures were determined to be 10.5, 10.9, 40.6, and 65.7 at 298 K, respectively, and which are 12.1, 12.9, 45.2, and 88.1 at 273 K (Figure 2f). The high selectivities for both C_3H_6 over C_2H_4 and C_2H_6/C_3H_8 over CH_4 suggest the promising potential of Zn-BPZ-SA for the separation and purification of MTO products, as well as natural gas.

Single-crystal diffraction is one of the most effective methods to understand the adsorption/separation mechanism. However, we were not able to obtain single-crystal data of activated Zn-BPZ-SA with absorbed gas molecules even after extensive attempts. To gain deep insights into the interactions between the framework and adsorbates, GCMC simulations were adopted to ascertain the preferential binding sites in Zn-BPZ-SA. It shows that the sites for C_2H_4, C_2H_6, C_3H_6, and C_3H_8 molecules are located at the corners of channels near the SA pillars. As given in Figure 3a, for C_2H_4, there are C−H···π and π···π interactions with the cyclobutenyl rings of SA as well as the methyl groups and pyrazolyl rings of HBPZ. The sites for C_2H_6 derive from the free O atoms of SA and pyrazolyl rings of HBPZ (Figure 3b). Compared to C_2H_4 and C_2H_6, C_3 hydrocarbons with a larger molecular size enhances the interactions with the framework. As shown in Figure 3c, C_3H_6 molecule interacts with one pyrazolyl, one cyclobutenyl, and uncoordinated one pyrazolyl N atom and one O atom of ligands to form stronger contacts including C−H···O/N/π and π···π interactions with distances of 2.786−3.408 Å. C_3H_8 also formed the multiple C−H···O/N/π interactions with the organic units in SA and HPBZ ligands (Figure 3d). For CH_4, although the CH_4 molecule can form two weak C−H···π contacts with the cyclobutenyl ring of SA ($H\cdots\pi_{centroid}$ = 3.141 and 3.146 Å), but the long separations of H···O = 3.30 Å and H···N = 3.59 Å between CH_4 and the O/N sites in the framework basically exclude the hydrogen bond interactions (Figure S19). Zn-BPZ-SA revealed the obviously higher binding energies for C_3H_8 (38.6 kJ mol^{-1}) and C_3H_6 (33.6 kJ mol^{-1}) than C_2H_6 (29.0 kJ mol^{-1}), C_2H_4 (22.6 kJ mol^{-1}), and CH_4 (18.2 kJ mol^{-1}), which reflects the stronger affinity toward C_3H_8 and C_3H_6, agreeing with the selective uptakes for C_3H_8 and C_3H_6. These simulation results are consistent with the differences in the polarizability of CH_4 (25.93×10^{-25} cm^3) < C_2H_4 (42.52×10^{-25} cm^3) < C_2H_6 ($44.3-44.7 \times 10^{-25}$ cm^3) < C_3H_6 (62.6×10^{-25} cm^3) < C_3H_8 ($62.9-63.7 \times 10^{-25}$ cm^3), as well as the same order of molecule sizes. The interactions are stronger for molecules which have larger size and polarizability, as reported in the literatures.[11,50]

The different binding sites in Zn-BPZ-SA for C_3H_6, C_2H_4, C_2H_6, and C_3H_8 at 298 K under 100 kPa were further investigated by simulations. As shown in Figure 4a−d, the MOF exhibits important three sites for C_3H_6 and C_3H_8 and two sites for C_2H_4 and C_2H_6. C_3H_8 and C_3H_6 molecules are involved in more contacts with the accessible sites of O/N atoms and π centers from ligands in pore wall, forming rich C−H···O/N/C hydrogen bonds and C−H···π or π···π interactions (Figure 4a, d). Notably, the methyl groups in HBPZ are also useful sites for C_3H_8 (C_3H_8−III) and C_3H_6 (C_3H_6−III) molecules through C−H···C interactions. By contrast, the interactions of the framework with both C_2H_6 and C_2H_4 are weak due to less contact fashions (Figure 4b,c). These findings are consistent

https://doi.org/10.1021/acsmaterialslett.3c00096
ACS Materials Lett. 2023, 5, 1091−1099

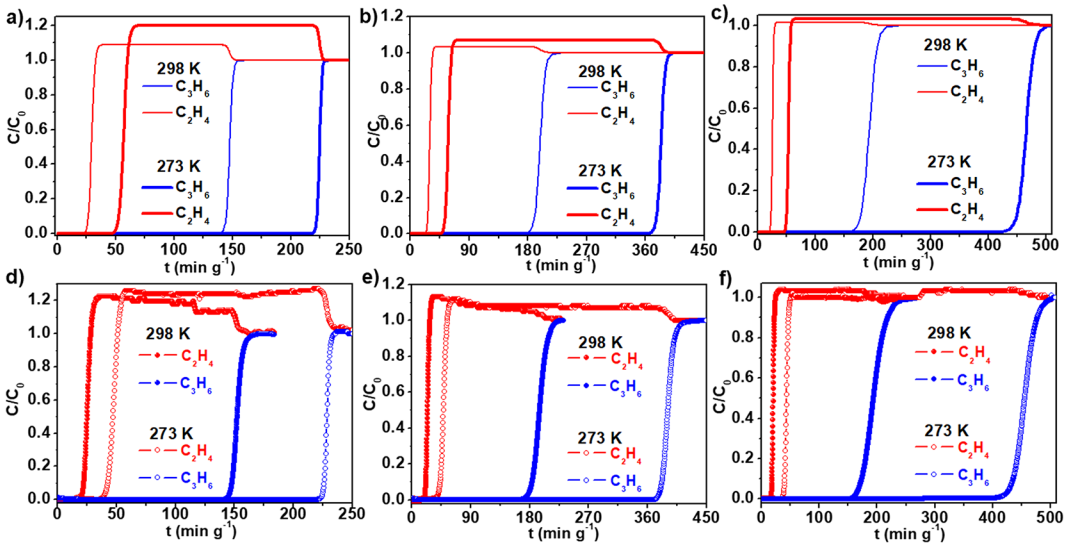

Figure 5. Simulated breakthrough curves of Zn-BPZ-SA for C_3H_6/C_2H_4 mixtures: (a) 50/50, (b) 20/50, and (c) 10/90; experimental breakthrough curves of Zn-BPZ-SA for C_3H_6/C_2H_4 mixtures: (d) 50/50, (e) 20/50, and (f) 10/90.

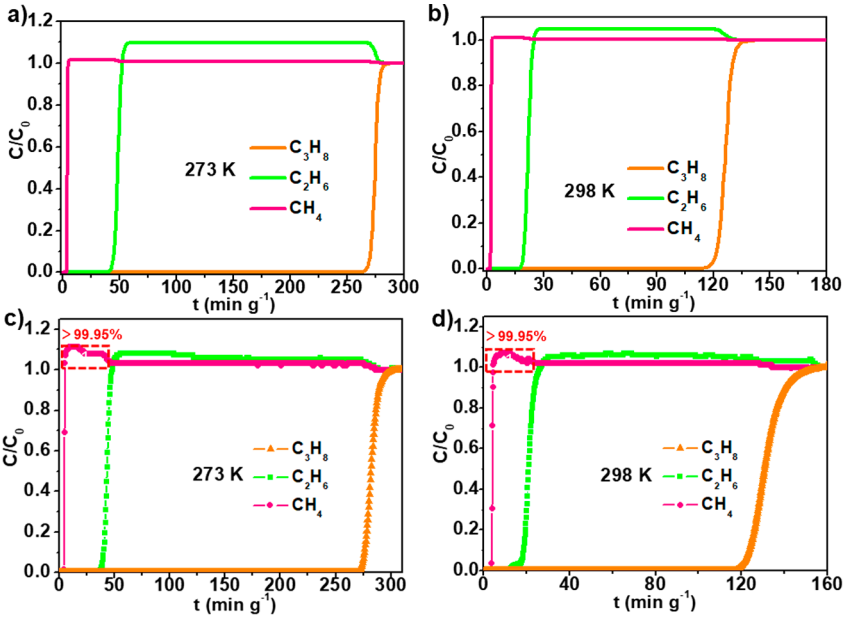

Figure 6. Simulated breakthrough curves of Zn-BPZ-SA for $C_3H_8/C_2H_6/CH_4$ mixtures (5/10/85) at 273 K (a) and 298 K (b); experimental breakthrough curves of Zn-BPZ-SA for $C_3H_8/C_2H_6/CH_4$ mixtures (5/10/85) at 273 K (c) and 298 K (d).

with the experimental selectivity of Zn-BPZ-SA for C_3 hydrocarbons over C_2 hydrocarbons.

To validate the feasibility using Zn-BPZ-SA to separate MTO products in a packed column, transient breakthrough simulations for C_3H_6/C_2H_4 (50/50, 20/50, and 10/90, v/v) mixtures were done at 273/298 K under 100 kPa using the methodology described by Krishna (see also Supporting Information).[51,52] The simulated curves in Figure 5a–c show that the mixtures were completely separated by Zn-BPZ-SA, whereby C_2H_4 breakthrough occurs first to yield the pure C_2H_4 but C_3H_6 passes through the column after longer times. Next, the actual separation performance was assessed by breakthrough experiments conducted on Zn-BPZ-SA at 298/273 K under 100 kPa, in which the ratios of 50/50, 20/50, and 10/90 C_3H_6/C_2H_4 mixtures with Ar as the carrier gas were respectively purged into a packed column (flow rate = 5.0 mL min^{-1}). Figure 5d–f shows that the measured curves excellently agree with the simulated results, in which C_3H_6 was preferentially adsorbed in the column, and C_2H_4 was first eluted with a high-purity >99.95% utill C_3H_6 broke through after substantial delay times of 143/222, 170/371, and 157/401 min g^{-1} for 50/50, 20/50, and 10/90 mixtures at 298/273 K, respectively. The corresponding breakthrough time differences (Δt) between C_3H_6 and C_2H_4 were 124/185, 153/333, and 143/365 min g^{-1} for three mixtures, far exceeding some benchmark materials, including spe-MOF,[36] iso-MOF-4,[7] CR-COF-1,[6] and CR-COF-2 (Figure S20).[6] The long Δt at both 298 and 273 K shows that the wide composite range of C_3H_6/C_2H_4 mixtures can be separated by Zn-BPZ-SA without precisely controlling temperature. During Δt, the collected high-grade C_2H_4 productivities (>99.95%), which were calculated on the basis of simulating experimental breakthrough were determined to be 21.9/39.3, 27.7/67.0, and

https://doi.org/10.1021/acsmaterialslett.3c00096
ACS Materials Lett. 2023, 5, 1091−1099

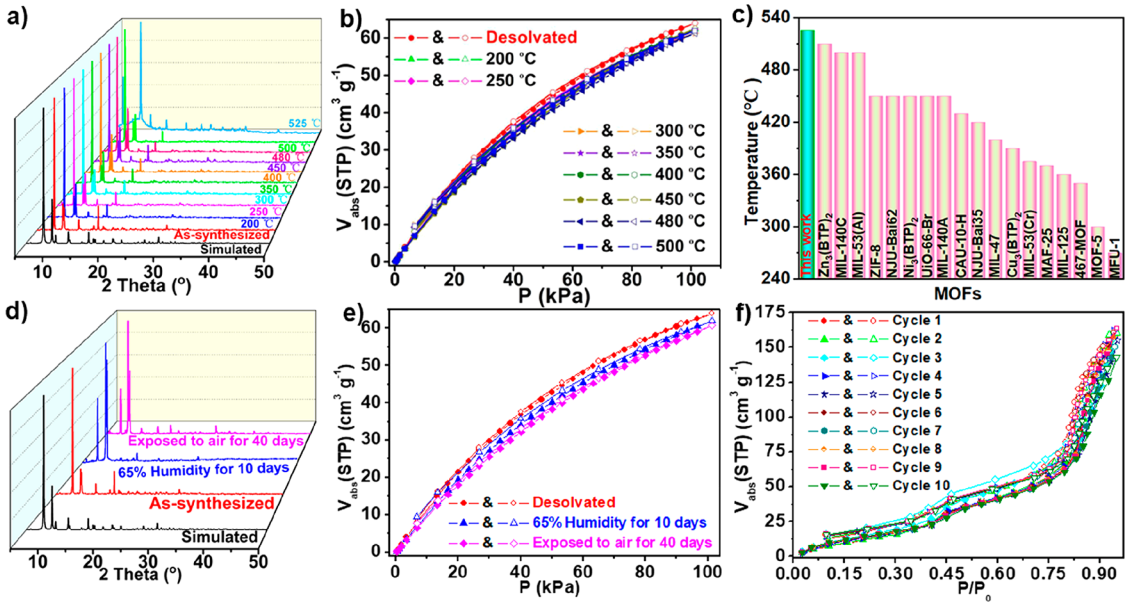

Figure 7. (a) PXRD patterns of Zn-BPZ-SA treated under different temperatures; (b) C_2H_4 sorption isotherms at 298 K of Zn-BPZ-SA treated under different temperatures; (c) comparison of the thermal stability among different MOFs; (d) PXRD patterns of Zn-BPZ-SA exposed to different environments; (e) C_2H_4 sorption isotherms at 298 K of Zn-BPZ-SA exposed to different environments; (f) water sorption isotherm cycles of Zn-BPZ-SA at 298 K.

51.5/142.8 L kg^{-1} for 50/50, 20/50, and 10/90 C_3H_6/C_2H_4 mixtures at 298/273 K, respectively. The productivities would be higher in industrial practice without the inert carrier gas. The identical breakthrough times for the multiple breakthrough experiments of C_3H_6/C_2H_4 mixtures confirmed great recyclability of material (Figure S21). Apparently, the desirable high-purity C_2H_4 can be directly obtained by separating MTO products through utilizing C_3H_6-selective MOFs, greatly increasing the separation efficiency.

The breakthrough curves of binary (C_2H_6/CH_4 and C_3H_8/CH_4) alkane mixtures with Ar as the carrier gas were also tested to evaluate the natural gas separation performance of Zn-BPZ-SA. As indicated in Figure S22a, b, when the C_2H_6/CH_4 (50/50 and 10/85, v/v) mixtures were fed into the packed column, CH_4 was eluted rapidly from the column, but C_2H_6 were detected until at 25.4/54.3 and 19.3/30.9 min g^{-1} for 50/50 and 10/85 mixtures at 298/273 K, respectively. Similar results were also observed in the breakthrough results of C_3H_8/CH_4 (50/50 and 5/85, v/v) mixtures, in which C_3H_8 was gauged at 147.5/299.1 and 180.4/524.4 min g^{-1} for 50/50 and 5/85 mixtures at 298/273 K, respectively (Figure S22c, d).

For natural gas purification, transient breakthrough simulations on Zn-BPZ-SA for $C_3H_8/C_2H_6/CH_4$ mixtures showed that CH_4 first flows out of the column since the weakest adsorption strength, which could thereby produce high-purity CH_4 before the C_2H_6 and C_3H_8 breakthrough occurred (Figure 6a, b). Experimental breakthrough curves of ternary 5/10/85 $C_3H_8/C_2H_6/CH_4$ (which roughly simulates the composition of natural gas) mixtures were also collected at 273 and 298 K (Figure 6c,d), which revealed remarkably similar results with the simulations. It shows that Zn-BPZ-SA can separate CH_4 from the ternary mixtures with significantly different breakthrough times. CH_4 was first eluted from the column to offer high-purity CH_4 (>99.95%) in the outlet until C_2H_6 broke through at 16.2/34.5 min g^{-1}, whereas C_3H_8 was retained with long times of 118.1/271.1 min g^{-1} in the column at 298/273 K. The productivities of ≥99.95% CH_4 purity calculated on the basis of breakthrough curves were determined to be 34.9 and 73.0 L kg^{-1} at 298 and 273 K, respectively, which are higher than that of LIFM-W2 and comparable to the reports in BSF-1, BSF-2, MIL-142A, and Ni(HBTC)(bipy),[15] suggesting the potential for CH_4 purification from natural gas. In addition, the cycling experiments of ternary mixtures further demonstrated the superior recyclability and stability of the material (Figure S23).

Zn-BPZ-SA also shows very high thermal stability, as measured by thermogravimetric analysis (TGA) that displays a wide thermostable flat in the range of 200−520 °C under N_2 atmosphere (Figure S24). The high thermostable temperature of the framework can be confirmed by the temperature-dependent PXRD tests (Figure 7a). The C_2H_4 adsorption isotherms of the sample after heating treatments agree well with those of the pristine material, further demonstrating remarkable thermal stability (Figure 7b). The thermal stability of Zn-BPZ-SA exceeds the reported major MOFs with high stable temperatures, including $Zn_3(BTP)_2$ (510 °C),[53] MIL-140c (500 °C),[54] ZIF-8 (500 °C),[55] and NJU-Bai62 (450 °C)[56] (Figure 7c, Table S5).

Considering the real environments of material in application, the resistance of Zn-BPZ-SA toward air and water humidity was evaluated. As shown in Figure 7d and 7e, after exposing Zn-BPZ-SA to the air for 40 days and relative humidity (65%) for 10 days, PXRD and C_2H_4 adsorption demonstrated excellent stability of the material. The water vapor sorption isotherm of Zn-BPZ-SA at 298 K exhibits a type-III curve (Figure 7f), in which the water uptake increases slowly before the pressure of P/P_0 = 0.8, and then rapidly, showing the hydrophobic feature of pores.[57,58] Most MOFs decreased or lost the water adsorption capacities after multiple cycles of water adsorption, however, Zn-BPZ-SA reveals repeated water sorption curves, which are very excellent compared to some representative MOFs, such as MOF-199 that lost 68% maximum uptake after five adsorption cycles.[59] The excellent thermal and water stability of Zn-BPZ-SA can be attributed to the utilization of methyl-functionalized dipyrazolate linkers, on one hand, the pyrazole junction with a large

https://doi.org/10.1021/acsmaterialslett.3c00096
ACS Materials Lett. 2023, 5, 1091−1099

pK_a value leads to robust M-N bonds, on the other hand, according to the coordinated environment of Zn^{2+} centers, one Zn^{2+} center is shielded by three methyl groups, which prevent the attack on the metal centers from water.[38,60]

Summarizing, we have synthesized a new MOF, Zn-BPZ-SA, with the multiple separation functions for MTO products and natural gas. The MOF with a layer-pillared network was constructed from judiciously selected methyl-functionalized pyrazole linkers and squaric acid pillars, possessing excellent resistance toward water, as well as exceptional thermal stability (520 °C). Zn-BPZ-SA reveals the high uptakes of 46.6 $cm^3\ g^{-1}$ for C_3H_6 and 48.0 $cm^3\ g^{-1}$ for C_3H_8 at the crucial low pressure of 10 kPa and preferential adsorption for C_3H_6 from C_3H_6/C_2H_4 mixtures, as well as selective captures for C_2H_6 and C_3H_8 from $C_3H_8/C_2H_6/CH_4$ mixtures, respectively. As a result, the MOF displayed efficient separation for MTO products of C_3H_6/C_2H_4 mixtures and also showed great separation performances for natural gas of $C_3H_8/C_2H_6/CH_4$ mixtures, affording the high-purity (>99.95%) C_2H_4 (21.9−142.8 L kg^{-1}) and CH_4 (34.9−73.0 L kg^{-1}) gases by one step, respectively. Molecular simulations highlighted the crucial roles of methyl groups and accessible active O/N sites in the pores of framework for separations. This presentation may contribute to the future development of advanced materials for achieving gas separation of light hydrocarbons.

■ ASSOCIATED CONTENT

Supporting Information

The Supporting Information is available free of charge at https://pubs.acs.org/doi/10.1021/acsmaterialslett.3c00096.

Synthesis of MOF; materials and general methods; X-ray crystallography; transient breakthrough simulations; breakthrough experiments; GCMC simulations, Q_{st} calculation; IAST selectivity calculation; SEM images; 3D structural figures; PXRD patterns; N_2 sorption isotherm; gas molecule parameters; preferential binding sites for CH_4; additional breakthrough curves; TGA curves; crystallographic data; selected bond lengths and bond angles; summary of adsorption capacity, Q_{st} value, selectivity, and thermal stability of different MOFs (PDF)

Crystallographic information file (CCDC 2212899) (CIF)

■ AUTHOR INFORMATION

Corresponding Author

Lei Hou − *Key Laboratory of Synthetic and Natural Functional Molecule of the Ministry of Education, Xi'an Key Laboratory of Functional Supramolecular Structure and Materials, College of Chemistry & Materials Science, Northwest University, Xi'an 710127, P. R. China;* orcid.org/0000-0002-2874-9326; Email: lhou2009@nwu.edu.cn

Authors

Gang-Ding Wang − *Key Laboratory of Synthetic and Natural Functional Molecule of the Ministry of Education, Xi'an Key Laboratory of Functional Supramolecular Structure and Materials, College of Chemistry & Materials Science, Northwest University, Xi'an 710127, P. R. China*

Rajamani Krishna − *Van 't Hoff Institute for Molecular Sciences, University of Amsterdam, 1098 XH Amsterdam, The Netherlands;* orcid.org/0000-0002-4784-8530

Yong-Zhi Li − *Key Laboratory of Synthetic and Natural Functional Molecule of the Ministry of Education, Xi'an Key Laboratory of Functional Supramolecular Structure and Materials, College of Chemistry & Materials Science, Northwest University, Xi'an 710127, P. R. China;* orcid.org/0000-0002-0297-5878

Yao-Yu Ma − *Key Laboratory of Synthetic and Natural Functional Molecule of the Ministry of Education, Xi'an Key Laboratory of Functional Supramolecular Structure and Materials, College of Chemistry & Materials Science, Northwest University, Xi'an 710127, P. R. China*

Yao-Yu Wang − *Key Laboratory of Synthetic and Natural Functional Molecule of the Ministry of Education, Xi'an Key Laboratory of Functional Supramolecular Structure and Materials, College of Chemistry & Materials Science, Northwest University, Xi'an 710127, P. R. China;* orcid.org/0000-0002-0800-7093

Zhonghua Zhu − *School of Chemical Engineering, The University of Queensland, Brisbane 4072, Australia;* orcid.org/0000-0003-2144-8093

Complete contact information is available at: https://pubs.acs.org/10.1021/acsmaterialslett.3c00096

Author Contributions

CRediT: **Gang-Ding Wang** data curation, writing-original draft; **Rajamani Krishna** formal analysis, software; **Yong-Zhi Li** formal analysis, investigation; **Yao-Yu Ma** methodology, visualization; **Lei Hou** funding acquisition, methodology, software, supervision, writing-review & editing; **Yao-Yu Wang** resources; **Zhonghua Zhu** software.

Notes

The authors declare no competing financial interest.

■ ACKNOWLEDGMENTS

This work is supported by NSFC (21871220 and 21971207).

■ REFERENCES

(1) Zhang, P.; Yang, L.; Liu, X.; Wang, J.; Suo, X.; Chen, L.; Cui, X.; Xing, H. Ultramicroporous material based parallel and extended paraffin nano-trap for benchmark olefin purification. *Nat. Commun.* **2022**, *13*, 4928.

(2) Lin, J. Y. S. Molecular sieves for gas separation. *Science* **2016**, *353*, 121−122.

(3) Hu, P.; Hu, J.; Liu, H.; Wang, H.; Zhou, J.; Krishna, R.; Ji, H. Quasi-Orthogonal Configuration of Propylene within a Scalable Metal-Organic Framework Enables Its Purification from Quinary Propane Dehydrogenation Byproducts. *ACS Cent. Sci.* **2022**, *8*, 1159−1168.

(4) Zhu, B.; Cao, J.-W.; Mukherjee, S.; Pham, T.; Zhang, T.; Wang, T.; Jiang, X.; Forrest, K. A.; Zaworotko, M. J.; Chen, K.-J. Pore Engineering for One-Step Ethylene Purification from a Three-Component Hydrocarbon Mixture. *J. Am. Chem. Soc.* **2021**, *143*, 1485−1492.

(5) Hu, P.; Han, J.; Zhou, J.; Wang, H.; Xiong, C.; Liu, H.; Zhou, X.; Wang, Y.; Ji, H. Customized H-bonding acceptor and aperture chemistry within a metal-organic framework for efficient C_3H_6/C_3H_8 separation. *Chem. Eng. J.* **2021**, *426*, 131302.

(6) Han, X.-H.; Gong, K.; Huang, X.; Yang, J.-W.; Feng, X.; Xie, J.; Wang, B. Syntheses of Covalent Organic Frameworks via a One-Pot Suzuki Coupling and Schiff's Base Reaction for C_2H_4/C_3H_6 Separation. *Angew. Chem., Int. Ed.* **2022**, *61*, e202202912.

(7) Fan, W.; Wang, X.; Zhang, X.; Liu, X.; Wang, Y.; Kang, Z.; Dai, F.; Xu, B.; Wang, R.; Sun, D. Fine-Tuning the Pore Environment of the Microporous Cu-MOF for High Propylene Storage and Efficient Separation of Light Hydrocarbons. *ACS Cent. Sci.* **2019**, *5*, 1261−1268.

(8) Sholl, D. S.; Lively, R. P. Seven chemical separations to change the world. *Nature* **2016**, *532*, 435−437.

(9) Liu, Y.; Chen, Z.; Liu, G.; Belmabkhout, Y.; Adil, K.; Eddaoudi, M.; Koros, W. Conformation-Controlled Molecular Sieving Effects for Membrane-Based Propylene/Propane Separation. *Adv. Mater.* **2019**, *31*, 1807513.
(10) Liu, X.; Hao, C.; Li, J.; Wang, Y.; Hou, Y.; Li, X.; Zhao, L.; Zhu, H.; Guo, W. An anionic metal-organic framework: metathesis of zinc(ii) with copper(ii) for efficient C_3/C_2 hydrocarbon and organic dye separation. *Inorg. Chem. Front.* **2018**, *5*, 2898−2905.
(11) Zheng, F.; Chen, R.; Zhang, Z.; Yang, Q.; Yang, Y.; Ren, Q.; Bao, Z. Cooperative control of intralayer and interlayer space in MOFs enables selective capture of intermediate-sized molecules. *Cell Rep. Phys. Sci.* **2022**, *3*, 100903.
(12) Kumar, K. V.; Preuss, K.; Titirici, M.-M.; Rodríguez-Reinoso, F. Nanoporous Materials for the Onboard Storage of Natural Gas. *Chem. Rev.* **2017**, *117*, 1796−1825.
(13) Han, G.; Wang, K.; Peng, Y.; Zhang, Y.; Huang, H.; Zhong, C. Enhancing Higher Hydrocarbons Capture for Natural Gas Upgrading by Tuning van der Waals Interactions in *fcu*-Type Zr-MOFs. *Ind. Eng. Chem. Res.* **2017**, *56*, 14633−14641.
(14) Zhang, Q.; Lian, X.; Krishna, R.; Yang, S. Q.; Hu, T. L. An ultramicroporous metal-organic framework based on octahedral-like cages showing high-selective methane purification from a six-component $C_1/C_2/C_3$ hydrocarbons mixture. *Sep. Purif Technol.* **2023**, *304*, 122312.
(15) Zhou, J.; Ke, T.; Steinke, F.; Stock, N.; Zhang, Z.; Bao, Z.; He, X.; Ren, Q.; Yang, Q. Tunable Confined Aliphatic Pore Environment in Robust Metal-Organic Frameworks for Efficient Separation of Gases with a Similar Structure. *J. Am. Chem. Soc.* **2022**, *144*, 14322−14329.
(16) Zhou, S.; Shekhah, O.; Ramírez, A.; Lyu, P.; Abou-Hamad, E.; Jia, J.; Li, J.; Bhatt, P. M.; Huang, Z.; Jiang, H.; Jin, T.; Maurin, G.; Gascon, J.; Eddaoudi, M. Asymmetric pore windows in MOF membranes for natural gas valorization. *Nature* **2022**, *606*, 706−712.
(17) Chen, K.-J.; Madden, D. G.; Mukherjee, S.; Pham, T.; Forrest, K. A.; Kumar, A.; Space, B.; Kong, J.; Zhang, Q.-Y.; Zaworotko, M. J. Synergistic sorbent separation for one-step ethylene purification from a four-component mixture. *Science* **2019**, *366*, 241−246.
(18) Li, L.; Lin, R.-B.; Krishna, R.; Li, H.; Xiang, S.; Wu, H.; Li, J.; Zhou, W.; Chen, B. Ethane/ethylene separation in a metal-organic framework with iron-peroxo sites. *Science* **2018**, *362*, 443−446.
(19) Datta, S. J.; Mayoral, A.; Murthy Srivatsa Bettahalli, N.; Bhatt, P. M.; Karunakaran, M.; Carja, I. D.; Fan, D.; Graziane M. Mileo, P.; Semino, R.; Maurin, G.; Terasaki, O.; Eddaoudi, M. Rational design of mixed-matrix metal-organic framework membranes for molecular separations. *Science* **2022**, *376*, 1080−1087.
(20) Wang, K.; Li, Y.; Xie, L.-H.; Li, X.; Li, J.-R. Construction and application of base-stable MOFs: a critical review Check for updates. *Chem. Soc. Rev.* **2022**, *51*, 6417−6441.
(21) Si, G.-R.; Wu, W.; He, T.; Xu, Z.-C.; Wang, K.; Li, J.-R. Stable Bimetallic Metal-Organic Framework with Dual-Functional Pyrazolate-Carboxylate Ligand: Rational Construction and C_2H_2/CO_2 Separation. *ACS Materials Lett.* **2022**, *4*, 1032−1036.
(22) Xiao, L.; Wang, Z.; Guan, J. 2D MOFs and their derivatives for electrocatalytic applications: Recent advances and new challenges. *Coord. Chem. Rev.* **2022**, *472*, 214777.
(23) Wang, J.; Zhang, Y.; Ma, Y.; Yin, J.; Wang, Y.; Fan, Z. Electrocatalytic Reduction of Carbon Dioxide to High-Value Multi-carbon Products with Metal-Organic Frameworks and Their Derived Materials. *ACS Materials Lett.* **2022**, *4*, 2058−2079.
(24) Liu, Q.; Wu, B.; Li, M.; Huang, Y.; Li, L. Heterostructures Made of Upconversion Nanoparticles and Metal-Organic Frameworks for Biomedical Applications. *Adv. Sci.* **2022**, *9*, 2103911.
(25) Ajoyan, Z.; Mandl, G. A.; Donnarumma, P. R.; Quezada-Novoa, V.; Bicalho, H. A.; Titi, H. M.; Capobianco, J. A.; Howarth, A. J. Modulating Photo- and Radioluminescence in Tb(III) Cluster-Based Metal-Organic Frameworks. *ACS Materials Lett.* **2022**, *4*, 1025−1031.
(26) Dong, Q.; Huang, Y.; Hyeon-Deuk, K.; Chang, I.-Y.; Wan, J.; Chen, C.; Duan, J.; Jin, W.; Kitagawa, S. Shape- and Size-Dependent Kinetic Ethylene Sieving from a Ternary Mixture by a Trap-and-Flow Channel Crystal. *Adv. Funct. Mater.* **2022**, *32*, 2203745.
(27) He, T.; Kong, X.-J.; Bian, Z.-X.; Zhang, Y.-Z.; Si, G.-R.; Xie, L.-H.; Wu, X.-Q.; Huang, H.; Chang, Z.; Bu, X.-H.; Zaworotko, M. J.; Nie, Z.-R.; Li, J.-R. Trace removal of benzene vapour using double-walled metal-dipyrazolate frameworks. *Nat. Mater.* **2022**, *21*, 689−695.
(28) Wang, Y.; Fu, M.; Zhou, S.; Liu, H.; Wang, X.; Fan, W.; Liu, Z.; Wang, Z.; Li, D.; Hao, H.; Lu, X.; Hu, S.; Sun, D. Guest-molecule-induced self-adaptive pore engineering facilitates purification of ethylene from ternary mixture. *Chem.* **2022**, *8*, 3263−3274.
(29) Zhang, B.; Rao, Y.; Hou, L.; Liu, B.; Li, Q. A Multinary Metal-Organic Framework with Divided Linkers for C_2H_2/CO_2 Separation. *ACS Materials Lett.* **2022**, *4*, 1774−1779.
(30) Zeng, H.; Xie, M.; Wang, T.; Wei, R.-J.; Xie, X.-J.; Zhao, Y.; Lu, W.; Li, D. Orthogonal-array dynamic molecular sieving of propylene/propane mixtures. *Nature* **2021**, *595*, 542−548.
(31) Fan, W.; Ying, Y.; Peh, S. B.; Yuan, H.; Yang, Z.; Yuan, Y. D.; Shi, D.; Yu, X.; Kang, C.; Zhao, D. Multivariate Polycrystalline Metal-Organic Framework Membranes for CO_2/CH_4 Separation. *J. Am. Chem. Soc.* **2021**, *143*, 17716−17723.
(32) Cadiau, A.; Adil, K.; Bhatt, P. M.; Belmabkhout, Y.; Eddaoudi, M. A metal-organic framework-based splitter for separating propylene from propane. *Science* **2016**, *353*, 137−140.
(33) Peng, Y.-L.; Wang, T.; Jin, C.; Deng, C.-H.; Zhao, Y.; Liu, W.; Forrest, K. A.; Krishna, R.; Chen, Y.; Pham, T.; Space, B.; Cheng, P.; Zaworotko, M. J.; Zhang, Z. Efficient propyne/propadiene separation by microporous crystalline physiadsorbents. *Nat. Commun.* **2021**, *12*, 5768.
(34) Fan, W.; Yuan, S.; Wang, W.; Feng, L.; Liu, X.; Zhang, X.; Wang, X.; Kang, Z.; Dai, F.; Yuan, D.; Sun, D.; Zhou, H.-C. Optimizing Multivariate Metal-Organic Frameworks for Efficient C_2H_2/CO_2 Separation. *J. Am. Chem. Soc.* **2020**, *142*, 8728−8737.
(35) Gong, W.; Cui, H.; Xie, Y.; Li, Y.; Tang, X.; Liu, Y.; Cui, Y.; Chen, B. Efficient C_2H_2/CO_2 Separation in Ultramicroporous Metal-Organic Frameworks with Record C_2H_2 Storage Density. *J. Am. Chem. Soc.* **2021**, *143*, 14869−14876.
(36) Fang, H.; Zheng, B.; Zhang, Z.-H.; Li, H.-X.; Xue, D.-X.; Bai, J. Ligand-Conformer-Induced Formation of Zirconium-Organic Framework for Methane Storage and MTO Product Separation. *Angew. Chem., Int. Ed.* **2021**, *60*, 16521−16528.
(37) DeCoste, J. B.; Peterson, G. W.; Jasuja, H.; Glover, T. G.; Huang, Y.; Walton, K. S. Stability and degradation mechanisms of metal-organic frameworks containing the $Zr_6O_4(OH)_4$ secondary building unit. *J. Mater. Chem. A* **2013**, *1*, 5642−5650.
(38) Wang, K.; Huang, H.; Xue, W.; Liu, D.; Zhao, X.; Xiao, Y.; Li, Z.; Yang, Q.; Wang, L.; Zhong, C. An ultrastable Zr metal-organic framework with a thiophene-type ligand containing methyl groups. *CrystEngComm* **2015**, *17*, 3586−3590.
(39) Gao, J.; Cai, Y.; Qian, X.; Liu, P.; Wu, H.; Zhou, W.; Liu, D.-X.; Li, L.; Lin, R.-B.; Chen, B. A Microporous Hydrogen-Bonded Organic Framework for the Efficient Capture and Purification of Propylene. *Angew. Chem., Int. Ed.* **2021**, *60*, 20400−20406.
(40) Yang, L.; Cui, X.; Ding, Q.; Wang, Q.; Jin, A.; Ge, L.; Xing, H. Polycatenated Molecular Cage-Based Propane Trap for Propylene Purification with Recorded Selectivity. *ACS Appl. Mater. Interfaces* **2020**, *12*, 2525−2530.
(41) Peng, Y.-L.; Wang, T.; Jin, C.; Li, P.; Suepaul, S.; Beemer, G.; Chen, Y.; Krishna, R.; Cheng, P.; Pham, T.; Space, B.; Zaworotko, M. J.; Zhang, Z. A robust heterometallic ultramicroporous MOF with ultrahigh selectivity for propyne/propylene separation. *J. Mater. Chem. A* **2021**, *9*, 2850−2856.
(42) Yang, S.-Q.; Sun, F.-Z.; Krishna, R.; Zhang, Q.; Zhou, L.; Zhang, Y.-H.; Hu, T.-L. Propane-Trapping Ultramicroporous Metal-Organic Framework in the Low-Pressure Area toward the Purification of Propylene. *ACS Appl. Mater. Interfaces* **2021**, *13*, 35990−35996.
(43) Xie, Y.; Shi, Y.; Cui, H.; Lin, R.-B.; Chen, B. Efficient Separation of Propylene from Propane in an Ultramicroporous Cyanide-Based Compound with Open Metal Sites. *Small Struct.* **2022**, *3*, 2100125.
(44) Pei, J.; Wen, H.-M.; Gu, X.-W.; Qian, Q.-L.; Yang, Y.; Cui, Y.; Li, B.; Chen, B.; Qian, G. Dense Packing of Acetylene in a Stable and Low-

https://doi.org/10.1021/acsmaterialslett.3c00096
ACS Materials Lett. 2023, 5, 1091−1099

Cost Metal-Organic Framework for Efficient C_2H_2/CO_2 Separation. *Angew. Chem., Int. Ed.* **2021**, *60*, 25068−25074.
(45) Qazvini, O. T.; Babarao, R.; Shi, Z.-L.; Zhang, Y.-B.; Telfer, S. G. A Robust Ethane-Trapping Metal-Organic Framework with a High Capacity for Ethylene Purification. *J. Am. Chem. Soc.* **2019**, *141*, 5014−5020.
(46) Zeng, H.; Xie, M.; Huang, Y.-L.; Zhao, Y.; Xie, X.-J.; Bai, J.-P.; Wan, M.-Y.; Krishna, R.; Lu, W.; Li, D. Induced Fit of C_2H_2 in a Flexible MOF Through Cooperative Action of Open Metal Sites. *Angew. Chem., Int. Ed.* **2019**, *58*, 8515−8519.
(47) Geng, D.; Zhang, M.; Hang, X.; Xie, W.; Qin, Y.; Li, Q.; Bi, Y.; Zheng, Z. A 2D metal-thiacalix[4]arene porous coordination polymer with 1D channels: gas absorption/separation and frequency response. *Dalton Trans.* **2018**, *47*, 9008−9013.
(48) Wu, X.; Bao, Z.; Yuan, B.; Wang, J.; Sun, Y.; Luo, H.; Deng, S. Microwave synthesis and characterization of MOF-74 (M = Ni, Mg) for gas separation. *Microporous Mesoporous Mater.* **2013**, *180*, 114−122.
(49) Fan, W.; Wang, Y.; Zhang, Q.; Kirchon, A.; Xiao, Z.; Zhang, L.; Dai, F.; Wang, R.; Sun, D. An Amino-Functionalized Metal-Organic Framework, Based on a Rare $Ba_{12}(COO)_{18}(NO_3)_2$ Cluster, for Efficient $C_3/C_2/C_1$ Separation and Preferential Catalytic Performance. *Chem. Eur. J.* **2018**, *24*, 2137−2143.
(50) Liu, Y.; Xu, Q.; Chen, L.; Song, C.; Yang, Q.; Zhang, Z.; Lu, D.; Yang, Y.; Ren, Q.; Bao, Z. Hydrogen-bonded metal-nucleobase frameworks for highly selective capture of ethane/propane from methane and methane/nitrogen separation. *Nano Res.* **2022**, *15*, 7695−7702.
(51) Krishna, R. Screening metal-organic frameworks for mixture separations in fixed-bed adsorbers using a combined selectivity/capacity metric. *RSC Adv.* **2017**, *7*, 35724−35737.
(52) Krishna, R. Metrics for Evaluation and Screening of Metal-Organic Frameworks for Applications in Mixture Separations. *ACS Omega* **2020**, *5*, 16987−17004.
(53) Colombo, V.; Galli, S.; Choi, H. J.; Han, G. D.; Maspero, A.; Palmisano, G.; Masciocchi, N.; Long, J. R. High thermal and chemical stability in pyrazolate-bridged metal-organic frameworks with exposed metal sites. *Chem. Sci.* **2011**, *2*, 1311−1319.
(54) Guillerm, V.; Ragon, F.; Dan-Hardi, M.; Devic, T.; Vishnuvarthan, M.; Campo, B.; Vimont, A.; Clet, G.; Yang, Q.; Maurin, G.; Ferey, G.; Vittadini, A.; Gross, S.; Serre, C. A Series of Isoreticular, Highly Stable, Porous Zirconium Oxide Based Metal-Organic Frameworks. *Angew. Chem., Int. Ed.* **2012**, *51*, 9267.
(55) Park, K. S.; Ni, Z.; Cote, A. P.; Choi, J. Y.; Huang, R.; Uribe-Romo, F. J.; Chae, H. K.; O'Keeffe, M.; Yaghi, O. M. Exceptional chemical and thermal stability of zeolitic imidazolate frameworks. *Proc. Natl. Acad. Sci. U.S.A.* **2006**, *103*, 10186−10191.
(56) Gao, Y.; Zhang, M.; Chen, C.; Zhang, Y.; Gu, Y.; Wang, Q.; Zhang, W.; Pan, Y.; Ma, J.; Bai, J. A low symmetry cluster meets a low symmetry ligand to sharply boost MOF thermal stability. *Chem. Commun.* **2020**, *56*, 11985.
(57) Serre, C. Superhydrophobicity in Highly Fluorinated Porous Metal-Organic Frameworks. *Angew. Chem., Int. Ed.* **2012**, *51*, 6048−6050.
(58) Kusgens, P.; Rose, M.; Senkovska, I.; Frode, H.; Henschel, A.; Siegle, S.; Kaskel, S. Characterization of metal-organic frameworks by water adsorption. *Microporous Mesoporous Mater.* **2009**, *120*, 325−330.
(59) Chen, Y.; Wang, B.; Wang, X.; Xie, L.-H.; Li, J.; Xie, Y.; Li, J.-R. A Copper(II)-Paddlewheel Metal-Organic Framework with Exceptional Hydrolytic Stability and Selective Adsorption and Detection Ability of Aniline in Water. *ACS Appl. Mater. Interfaces* **2017**, *9*, 27027−27035.
(60) Sumida, K.; Rogow, D. L.; Mason, J. A.; McDonald, T. M.; Bloch, E. D.; Herm, Z. R.; Bae, T.-H.; Long, J. R. Carbon Dioxide Capture in Metal-Organic Frameworks. *Chem. Rev.* **2012**, *112*, 724−781.

https://doi.org/10.1021/acsmaterialslett.3c00096
ACS Materials Lett. 2023, 5, 1091−1099

Supporting Information

Rational Construction of Ultrahigh Thermal Stable MOF for Efficient Separation of MTO Products and Natural Gas

Gang-Ding Wang,[a] Rajamani Krishna,[b] Yong-Zhi Li,[a] Yao-Yu Ma,[a] Lei Hou,*[a] Yao-Yu Wang,[a] and Zhonghua Zhu[c]

[a]Key Laboratory of Synthetic and Natural Functional Molecule of the Ministry of Education, Xi'an Key Laboratory of Functional Supramolecular Structure and Materials, College of Chemistry & Materials Science, Northwest University, Xi'an 710127, P. R. China.

[b]Van 't Hoff Institute for Molecular Sciences, University of Amsterdam, Amsterdam 1098 XH, The Netherlands.

[c]School of Chemical Engineering, The University of Queensland, Brisbane 4072, Australia.

*To whom correspondence should be addressed. E-mail: lhou2009@nwu.edu.cn (Lei Hou).

Synthesis of Zn-BPZ-SA

The mixture containing 0.0297 g $Zn(NO_3)_2 \cdot 6H_2O$ (0.1 mmol), 0.019 g H_2BPZ (0.1 mmol), 0.0114 g H_2SA (0.1 mmol), and 3 mL DMF was sealed in a vessel (25 mL). The vessel was heated at 130 °C for 72 h, and then cooled to RT at a rate of 10 °C h^{-1} to give colorless bulk crystals (yield: 51%, based on $Zn(NO_3)_2 \cdot 6H_2O$). The sample morphology was characterized by SEM (Figure S1). Anal. Calcd for $C_{12.75}H_{20.75}ZnN_{4.25}O_{5.25}$: C, 39.98; H, 5.46; N, 15.54%. Found: C, 40.12; H, 5.13; N, 15.31%.

Materials and General Methods

The reagents were purchased commercially. Elemental analyses were determined with a Perkin-Elmer 2400C elemental analyzer. Thermalgravimetric analyses (TGA) were tested in a nitrogen stream using a Netzsch TG209F3 equipment (10 °C min^{-1}). Powder X-ray diffraction (PXRD) data were recorded on a Bruker D8 ADVANCE X-ray powder diffractometer (Cu Kα, λ = 1.5418 Å). Single crystal diffraction data were collected on a Bruker SMART APEX II CCD diffractometer. The product morphology was tested by a field emission scanning electron microscope (FESEM S-8010 Hitachi) with an acceleration voltage of 20 kV. Sorption measurements were performed with an automatic volumetric sorption apparatus (Micrometrics ASAP 2020M and TriStar II 3020), in which the sample was activated by immersing in CH_2Cl_2 for 72 hours and then heating at 393 K under vacuum for 4 hours. Breakthrough experiments were performed on a Quantachrome dynaSorb BT equipment.

X-Ray Crystallography

A Bruker Smart Apex II CCD detector was used to collect the single crystal data at 150(2) K using graphite-monochromated Ga Kα (λ = 1.34139 Å). The structure was solved by direct methods and refined by full-matrix least-squares refinement based F^2 with the SHELXTL program. The non-hydrogen atoms were refined anisotropically with the hydrogen atoms added at their geometrically ideal positions and refined isotropically. As the disordered solvent molecules in the structure cannot be located, the SQUEEZE routine of Platon program was applied in refining. The formula of complex was get by the single crystal analysis together with elemental microanalyses and TGA data. Relevant crystallographic

results are listed in Table S1. Selected bond lengths and angles are provided in Table S2.

Transient Breakthrough Simulations

Transient breakthrough simulations were carried out for the same set of operating conditions as in the experimental data sets, using the methodology described in earlier publications.[1-5] In these simulations, intra-crystalline diffusion influences are ignored. For Zn-BPZ-SA, there is excellent match between the experiments and simulations. From the simulations on the experimental breakthrough curves, the productivities of 99.95% pure C_2H_4 and 99.95% pure CH_4 were determined; these are expressed in the units of L per kg of MOF.

Breakthrough Experiments

The breakthrough experiment was performed on the Quantachrome dynaSorb BT equipments at 298 K and 1 bar with Ar as the carrier gas. The activated Zn-BPZ-SA (about 0.8 g) was filled into a packed column of ϕ 4.2 mm × 80 mm, and then the packed column was washed with Ar at a rate of 7 mL min^{-1} at 343 K for 30 minutes to further activate the samples. Between two breakthrough experiments, the adsorbent was regenerated by Ar flow of 7 mL min^{-1} for 35 min at 343 K to guarantee a complete removal of the adsorbed gas.

GCMC Simulations

Grand canonical Monte Carlo (GCMC) simulations were performed for the gas adsorption in the framework by the Sorption module of Material Studio (Accelrys. Materials Studio Getting Started). The framework was considered to be rigid, and the optimized gas molecules were used. The atom charges and bond lengths for the gas molecules are shown in Figure S18. The partial charges for atoms of the framework were derived from QEq method and QEq neutral 1.0 parameter. One unit cell was used during the simulations. The interaction energies between the gas molecules and framework were computed through the Coulomb and Lennard-Jones 6-12 (LJ) potentials. All parameters for the atoms were modeled with the universal force field (UFF) embedded in the MS modeling package. A cutoff distance of 12.5 Å was used for LJ interactions, and the Coulombic interactions were calculated by using Ewald summation. For each run, the 3×10^6 maximum loading steps, 3×10^6 production steps were employed.

The binding energy was calculated by Castep software. The exchange-correlation

functional used in calculations was in the framework of the generalized gradient approximation (GGA) proposed by Perdew, Burke and Ernzerhof (PBE). DNP basis set was used to describe the atomic orbital. The binding energy is evaluated by the following equation: $E_{bind} = E_{framework+gas} - E_{framework} - E_{gas}$, in which $E_{framework+gas}$ is the total energy of the framework and the adsorbed gas molecule, $E_{framework}$ and E_{gas} are the energies of the framework and gas molecule.

Fitting Adsorption Heat of Pure Component Isotherms

$$\ln P = \ln N + 1/T \sum_{i=0}^{m} a_i N^i + \sum_{i=0}^{n} b_i N^i \qquad Q_{st} = -R \sum_{i=0}^{m} a_i N^i$$

The virial equation was used to fit the combined isotherm data for Zn-BPZ-SA at 273 and 298 K, where P is the pressure, N is the adsorbed amount, T is the temperature, a_i and b_i are virial coefficients, and m and N are the number of coefficients used to describe the isotherms. Q_{st} is the coverage-dependent heat of adsorption and R is the universal gas constant.

Gas Selectivity Prediction via IAST

The experimental isotherm data for pure gas were fitted using a dual Langmuir-Freundlich (L-F) model:

$$q = \frac{a_1 * b_1 * P^{c1}}{1 + b_1 * P^{c1}} + \frac{a_2 * b_2 * P^{c2}}{1 + b_2 * P^{c2}}$$

Where q and p are adsorbed amounts and the pressure of component i, respectively.

The adsorption selectivities for binary mixtures defined by

$$S_{i/j} = \frac{x_i * y_j}{x_j * y_i}$$

were respectively calculated using the Ideal Adsorption Solution Theory (IAST). Where xi is the mole fraction of component i in the adsorbed phase and yi is the mole fraction of component i in the bulk.

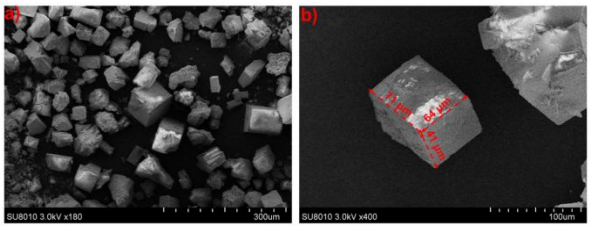

Figure S1. SEM image of Zn-BPZ-SA (a), and the image of the single crystal with the particle sizes of 71 μm × 64 μm × 41 μm (b).

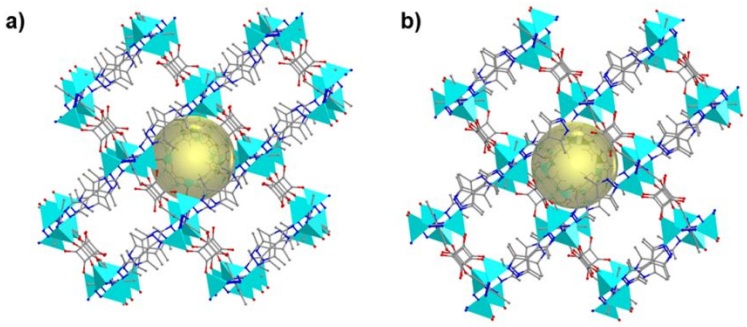

Figure S2. a) 3D framework of Zn-BPZ-SA viewed along the *a* axis; b) 3D framework of Zn-BPZ-SA viewed along the *b* axis.

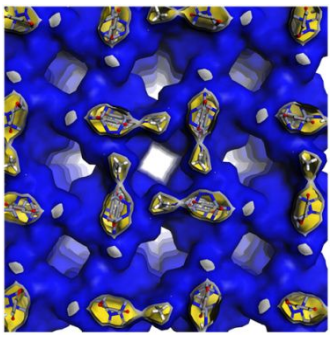

Figure S3. Accessible surface representation of pores in Zn-BPZ-SA viewed along the *c* axis.

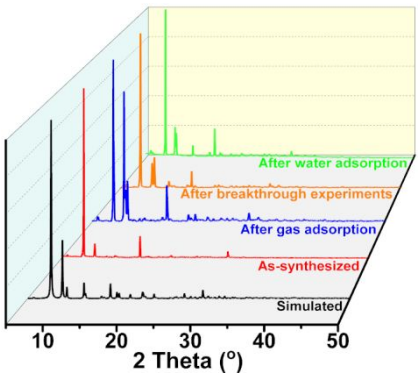

Figure S4. PXRD patterns of Zn-BPZ-SA.

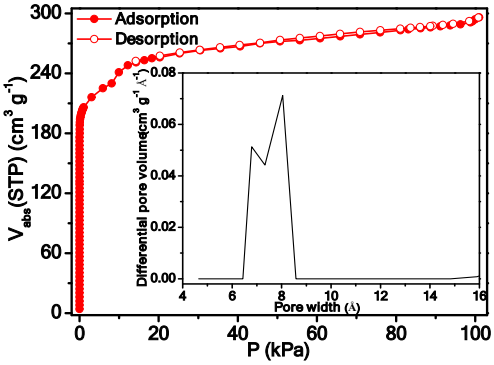

Figure S5. Adorption isotherm of Zn-BPZ-SA for N_2 at 77 K, and the insert shows the pore size distribution based on the density functional theory method.

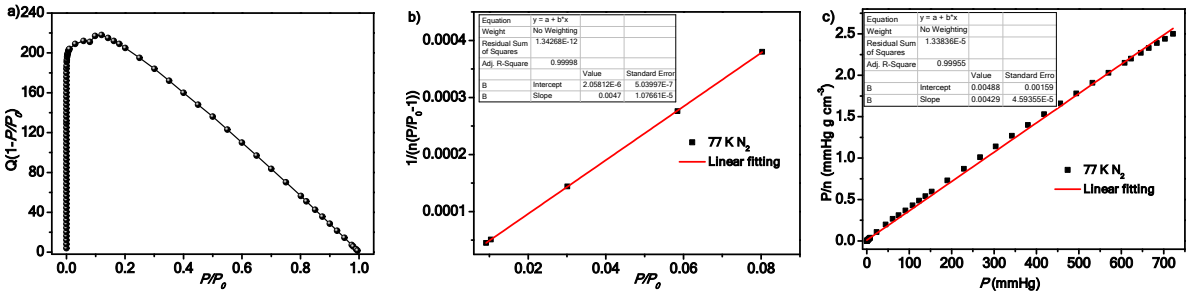

S_{BET} = 1/(2.05812E^{-6} + 0.0047)/22414 × 6.023 × 10^{23} × 0.162 × 10^{-18} =925 m^2 g^{-1}.

$S_{Langmuir}$ = (1/ 0.00429)/22414 × 6.023 × 10^{23} × 0.162 × 10^{-18} = 1013 m ^{2} g $^{-1}$

Figure S6. The consistency plot a), BET surface area plot b), and Langmuir surface area plot c) for Zn-BPZ-SA.

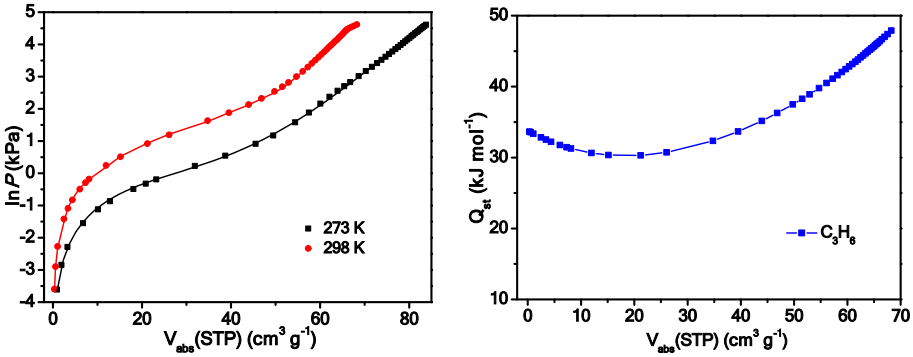

Figure S7. Fitted C_3H_6 isotherms of Zn-BPZ-SA, and the isosteric heats of adsorption (Q_{st}). Fitting results, a0 = -4063.42187, a1 = 49.96209, a2 = -1.69184, a3 = 0.01419, a4 = -0.00008, b0 = 11.25522, b1 = -0.13915, b2 = 0.0038, Chi^2 = 0.00194, R^2 = 0.99965.

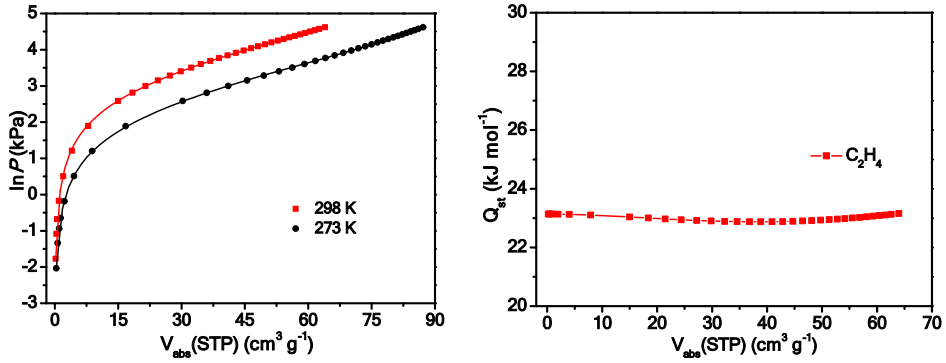

Figure S8. Fitted C_2H_4 isotherms of Zn-BPZ-SA, and the isosteric heats of adsorption (Q_{st}). Fitting results, a0 = -2783.04858, a1 = 0.00812, a2 = 0.0793, a3 = -0.00189, a4 = 0.00001, b0 = 9.21546, b1 = -0.00536, b2 = 0.00021, Chi^2 = 0.00021, R^2 = 0.99994.

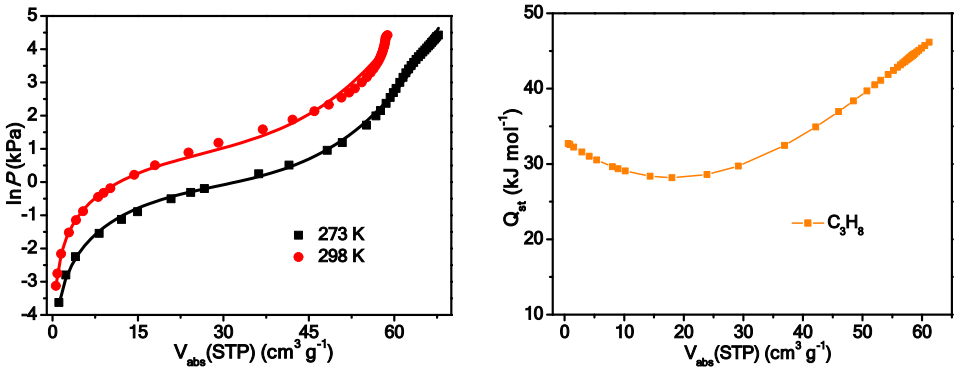

Figure S9. Fitted C_3H_8 isotherms of Zn-BPZ-SA, and the isosteric heats of adsorption (Q_{st}). Fitting results, a0 = -3974.76559, a1 = 66.87671, a2 = -1.99892, a3 = 0.00425, a4 = 0.00006, b0 = 10.70141, b1 = -0.19747, b2 = 0.00549, Chi^2 = 0.02023, R^2 = 0.99632.

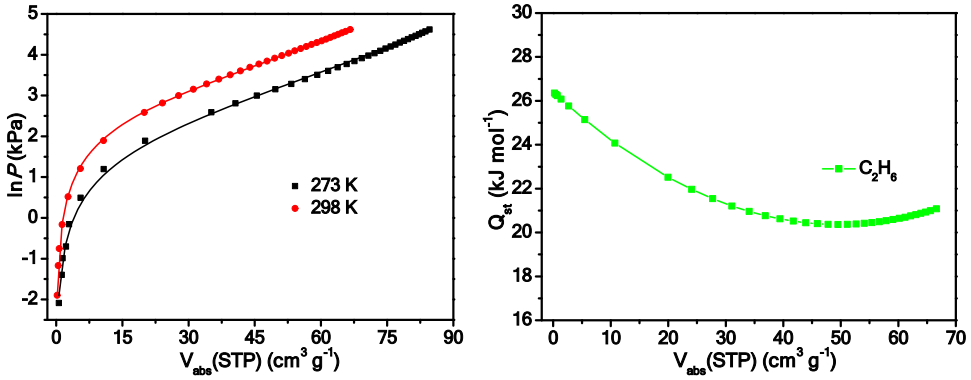

Figure S10. Fitted C_2H_6 isotherms of Zn-BPZ-SA, and the isosteric heats of adsorption (Q_{st}). Fitting results, a0 = -3175.95175, a1 = 29.29987, a2 = -0.29547, b0 = 10.21795, b1 = -0.10058, b2 = 0.00122, Chi^2 = 0.00328, R^2 = 0.99911.

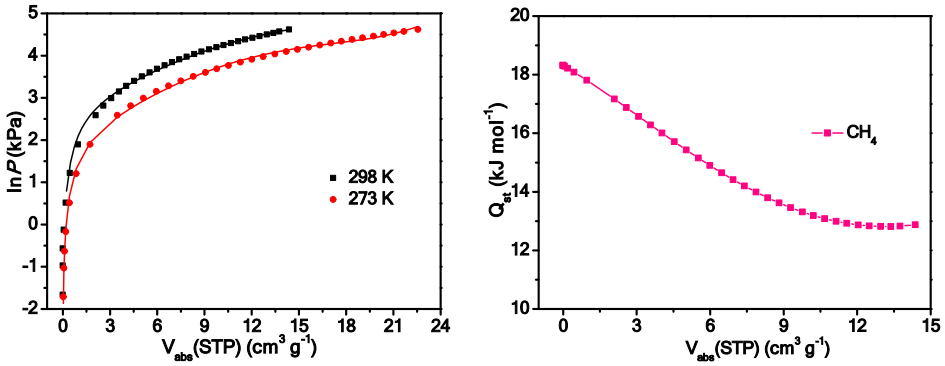

Figure S11. Fitted CH_4 isotherms of Zn-BPZ-SA, and the isosteric heats of adsorption (Q_{st}). Fitting results, a0 = -2202.9535, a1 = 59.45118, a2 = 4.21913, a3 = -0.51122, a4 = 0.01046, b0 = 9.67103, b1 = -0.38804, b2 = 0.01478, Chi^2 = 0.00845, R^2 = 0.99674.

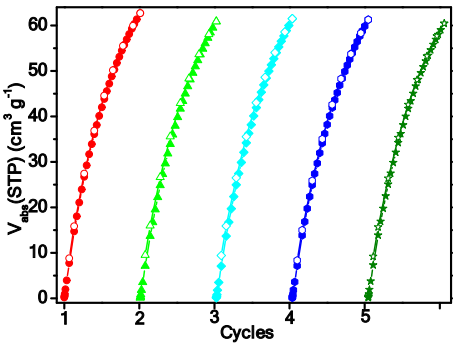

Figure S12. Adsorption cycles of Zn-BPZ-SA for C_2H_4 at 298 K.

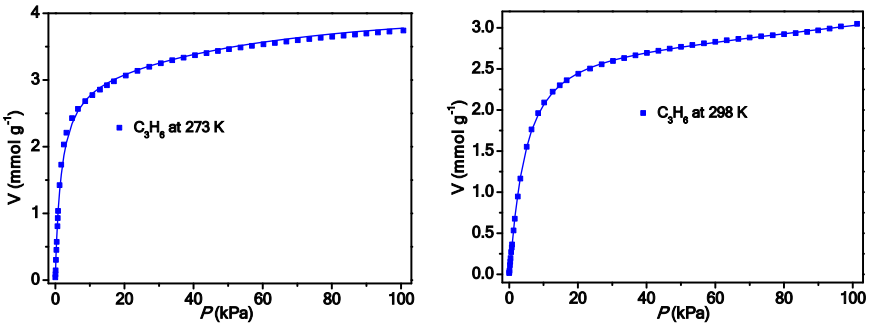

Figure S13. C_3H_6 adsorption isotherms of Zn-BPZ-SA with fitted by dual L-F model, 273 K: a1 = 3.29277, b1 = 0.55231, c1 = 0.94239, a2 = 0.79349, b2 = 0.0009, c2 = 1.71069, Chi^2 = 0.00346, R^2 = 0.99793; 298 K: a1 = 2.8572, b1 = 0.17641, c1 = 1.16641, a2 = 0.97179, b2 = 0.00001, c2 = 2.19626, Chi^2 = 0.00012, R^2 = 0.99991.

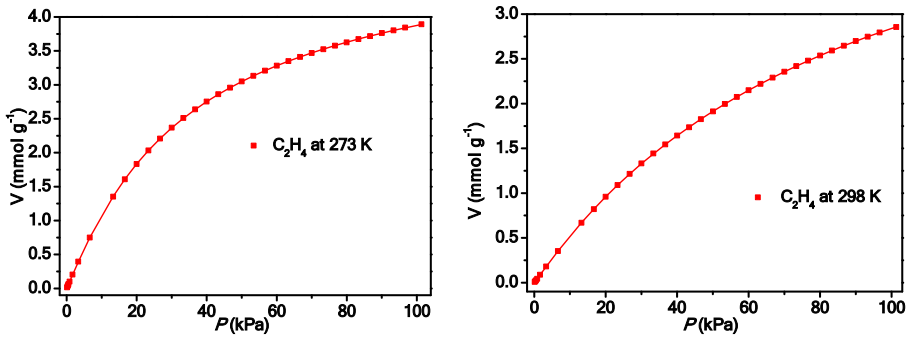

Figure S14. C_2H_4 adsorption isotherms of Zn-BPZ-SA with fitted by dual L-F model, 273 K: a1 = 3.71794, b1 = 0.0203, c1 = 1.16382, a2 = 2.59893, b2 = 0.01853, c2 = 0.71236, Chi^2 = 4.9459E-6, R^2 = 1; 298 K: a1 = 0.97457, b1 = 0.00025, c1 = 1.78347, a2 = 3.74181, b2 = 0.01395, c2 = 1.04771, Chi^2 = 2.0337E-6, R^2 = 1.

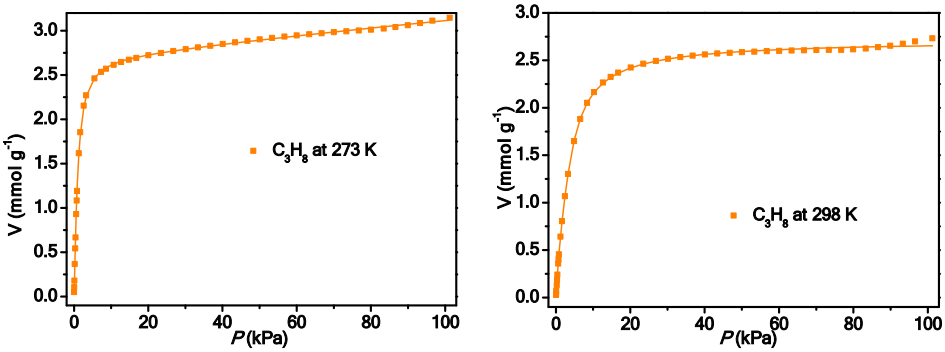

Figure S15. C_3H_8 adsorption isotherms of Zn-BPZ-SA with fitted by dual L-F model, 273 K: a1 = 2.69472, b1 = 1.06089, c1 = 1.30206, a2 = 2.89518, b2 = 0.00103, c2 = 1.11115, Chi^2 = 0.003, R^2 = 0.99971; 298 K: a1 = 0.43584, b1 = 0.02107, c1 = 2.66945, a2 = 2.27646, b2 = 0.29933, c2 = 1.04854, Chi^2 = 0.00033, R^2 = 0.9997.

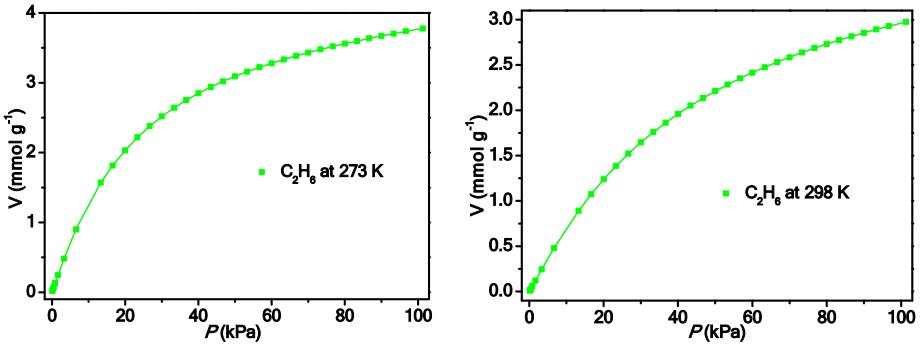

Figure S16. C_3H_8 adsorption isotherms of Zn-BPZ-SA with fitted by dual L-F model, 273 K: a1 = 2.69472, b1 = 1.06089, c1 = 1.30206, a2 = 2.89518, b2 = 0.00103, c2 = 1.11115, Chi^2 = 0.003, R^2 = 0.99971; 298 K: a1 = 0.43584, b1 = 0.02107, c1 = 2.66945, a2 = 2.27646, b2 = 0.29933, c2 = 1.04854, Chi^2 = 0.00033, R^2 = 0.9997.

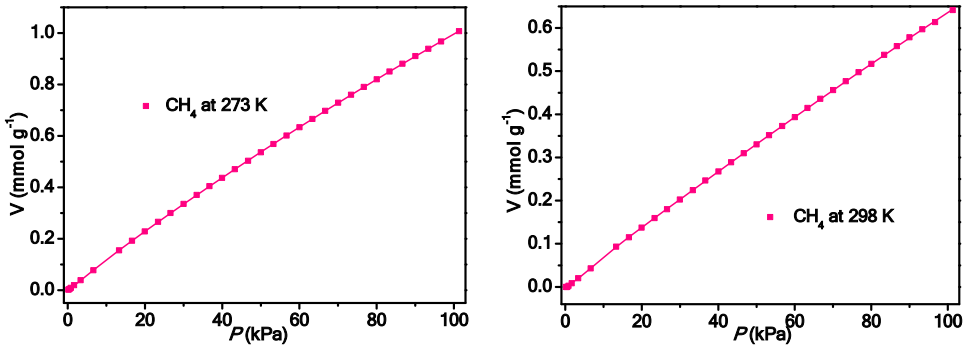

Figure S17. CH_4 adsorption isotherms of Zn-BPZ-SA with fitted by dual L-F model, 273 K: a1 = 6.53427, b1 = 0.00143, c1 = 1.04154, a2 = 0.03131, b2 = 0.03227, c2 = 1.50639, Chi^2 = 3.2368E-7, R^2 = 1; 298 K: a1 = 5.57644, b1 = 0.00095, c1 = 1.06026, a2 = 0.01458, b2 = 0.00079, c2 = 3.23975, Chi^2 = 1.4542E-6, R^2 = 0.99997.

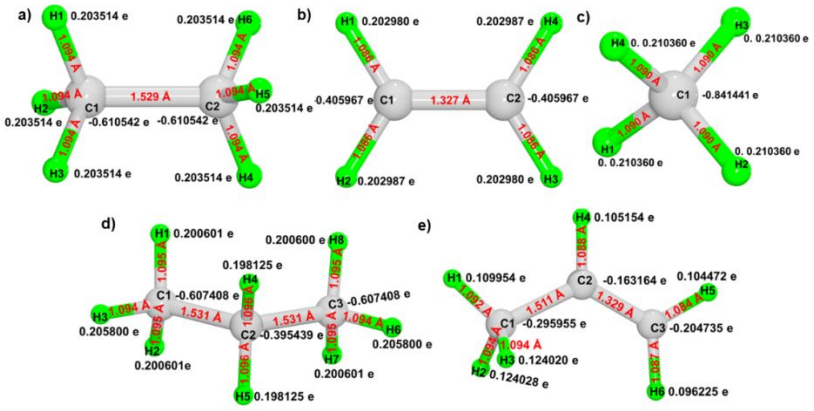

Figure S18. Bond lengths and atom charges in gas molecules in simulations, a) C_2H_6; b) C_2H_4; c) CH_4; d) C_3H_8; e) C_3H_6.

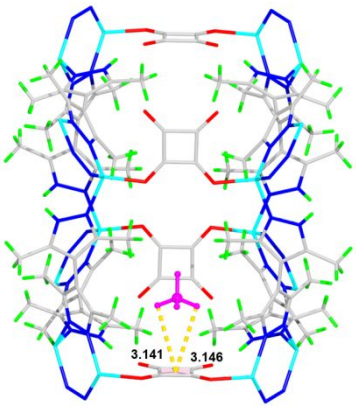

Figure S19. Preferential bingding sites for CH_4 in Zn-BPZ-SA, forming C-H···π interactions.

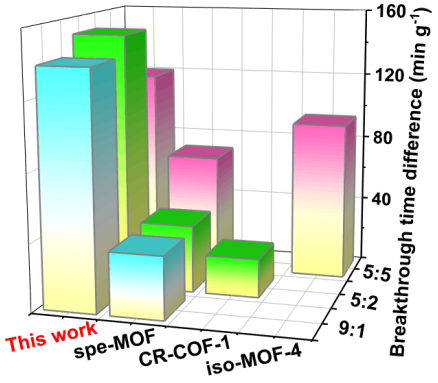

Figure S20. Comparison of breakthrough time differences for C_3H_6/C_2H_4 mixtures in porous materials.

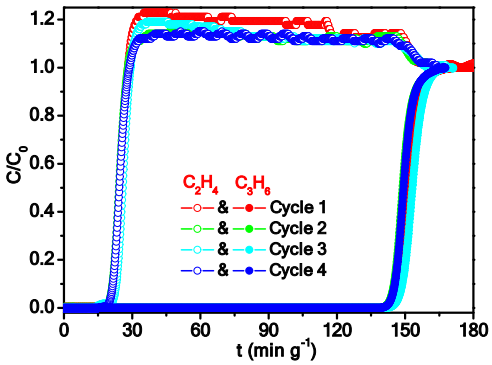

Figure S21. Breakthrough cycles of Zn-BPZ-SA for C_3H_6/C_2H_4 mixtures at 298 K.

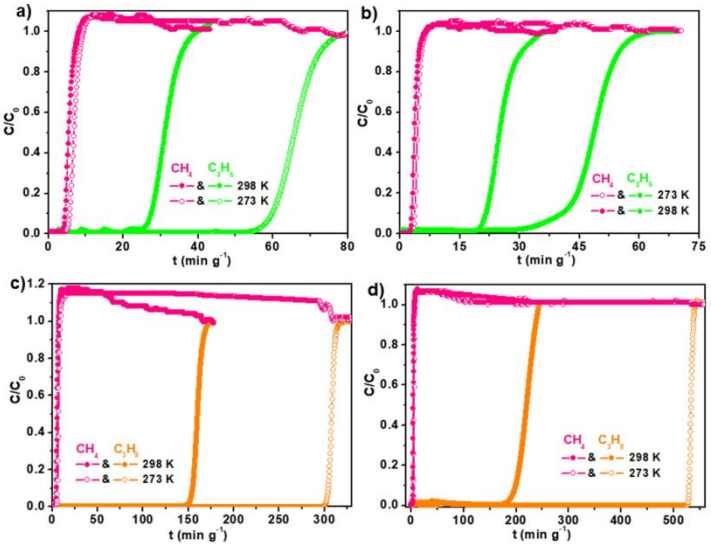

Figure S22. Breakthrough curves of Zn-BPZ-SA for C_2H_6/CH_4 mixtures: a) 50/50, b) 10/85; breakthrough curves of Zn-BPZ-SA for C_3H_8/CH_4 mixtures: c) 50/50, d) 5/85.

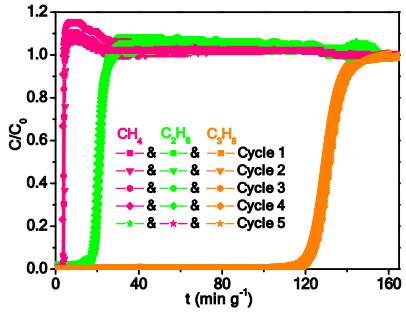

Figure S23. Breakthrough cycles of Zn-BPZ-SA for $C_3H_8/C_3H_6/CH_4$ mixtures at 298 K.

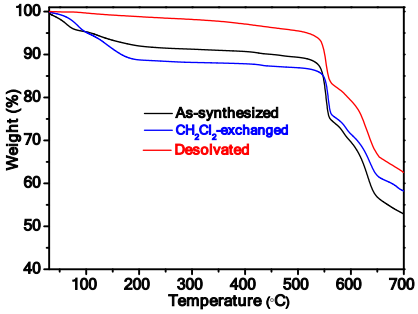

Figure S24. TGA curves of Zn-BPZ-SA.

Table S1. Crystal Data and Structure Refinements for Zn-BPZ-SA.

Chemical formula	$C_{12}H_{13}ZnN_4O_2$
Formula weight	310.63
T (K)	150(2)
Crystal system, space group	Tetragonal, I_4/m
a, b, c (Å)	21.4100(10), 21.4100(10), 17.9644(16)
α, β, γ (°)	90, 90, 90
V (Å^3), Z	8234.7(11), 16
Dcalcd. (g·cm^{-3}), μ (mm^{-1})	1.002, 1.109
Reflns collected/unique, R_{int}	28375/3899, 0.0395
Goof	1.033
$R_1{}^a$, $wR_2{}^b$ [$I > 2\sigma$]	$R_1 = 0.0801$, $wR_2 = 0.2202$
$R_1{}^a$, $wR_2{}^b$ (all data)	$R_1 = 0.0833$, $wR_2 = 0.2244$

$^aR_1 = \Sigma(|F_o|-|F_c|)/\Sigma|F_o|$. $^bR_2 = [\Sigma w(F_o^2 - F_c^2)^2/\Sigma w(F_o^2)^2]^{1/2}$.

Table S2. Selected bond lengths (Å) and bond angles (deg) for Zn-BPZ-SA.

Zn(1)-O(1)	1.933(4)	O(1)-Zn(1)-N(2)$^{\#1}$	111.6(2)
Zn(1)-N(1)	1.958(4)	O(1)-Zn(1)-N(3)$^{\#2}$	103.63(17)
Zn(1)-N(2)$^{\#1}$	1.962(5)	N(1)-Zn(1)-N(2)$^{\#1}$	114.92(17)
Zn(1)-N(3)$^{\#2}$	2.017(4)	N(1)-Zn(1)-N(3)$^{\#2}$	109.2(2)
O(1)-Zn(1)-N(1)	110.7(2)	N(2)$^{\#1}$-Zn(1)-N(3)$^{\#2}$	106.0(2)

Symmetry codes: #1 -x+1/2, -y+1/2, -z+1/2; #2 -y+1/2, x-1/2, -z+1/2.

Table S3. Summary of adsorption capacity and Q_{st} value of C_3H_6 and C_2H_4 and C_3H_6/C_2H_4 and selectivity for different MOFs at 298 K under 100 kPa.

MOF	$Q_{st,\ propylene}$ (kJ mmol^{-1})	$Q_{st,\ ethylene}$ (kJ mmol^{-1})	$q_{propylene}$ (cm^3 g^{-1})		$q_{ethylene}$ (cm^3 g^{-1})	Selectivity (v/v)			Ref.
			10 kPa	100 kPa	100 kPa	1:1	2:5	1:9	
Zn-BPZ-SA	33.65	23.13	46.6	68.3	63.9	4.8	5.3	6.1	This work
NEM-7-Cu	36.9	22.5	25	75.5	29	8.6	NA	NA	6
UPC-33	48.93	10.31	24	94.3	31.1	5.7	NA	5.84	7
CR-COF-1	29.8	26	35.6	84	38	NA	NA	NA	8
iso-MOF-4	30.9	25.4	NA	254.5	73	5.08	NA	5.36	9
spe-MOF	29.6	22.5	30	236.9	48.9	7.7	7.0	6.7	10
LIFM-38	27.3	28.1	15.5	58	20	6.4	NA	NA	11
PCP **1'**	14.8	24.7	38.1	70.67	55.67	3.6	NA	NA	12
$[Cd_2(AzDC)_2(TPT)_2](DMF)_3$	42.1	30.6	35.2	59.84	44.95	1.2	NA	NA	13

*NA = not available

Table S4. Summary of adsorption capacity and Q_{st} value of C_3H_8 and C_2H_6 and C_3H_8/C_2H_6 selectivity for different MOFs at 298 K under 100 kPa.

MOF	$Q_{st,\ propane}$ (kJ mmol^{-1})	$Q_{st,\ ethane}$ (kJ mmol^{-1})	$q_{propane}$ (cm^3 g^{-1})	q_{ethane} (cm^3 g^{-1})	Selectivity (v/v, 1:1)	Ref.
			100 kPa	100 kPa		
Zn-BPZ-SA	32.7	26.4	61.2	66.6	4.3	This work
$Ni(4\text{-}DPDS)_2CrO_4$	65.2	41.6	34.6	33.4	5.88	14
UPC-33	18.39	13.86	93.6	35	4.88	7
LIFM-38	28.3	28.5	55	24	5.1	11
PCP **1'**	21.8	27.3	64.6	64.0	4.5	12
$[Cd_2(AzDC)_2(TPT)_2]$	40.8	34.2	60.65	45.74	0.43	13
Cu-MOF	40.7	15.6	134.0	72.2	NA	15
PAN-2(CF_3)	41.7	35.6	102.6	79.1	6.5	16
PAN-5H	35.7	28.7	81.3	52.6	8.4	16
PAN-5F	33.0	26.7	43.9	29.1	9.4	16
PAN-2F	41.1	36.7	103.5	81.5	7.2	16
SNNU-Bai68	38.6	33.6	71.8	65	3.4	17

*NA = not available

Table S5. Summary of the thermal stability for different MOFs.

MOF	Ligand	SBU	BET surface area (m^2 g^{-1})	Thermal stability	Ref.
MFU-4l	H_2-BTDD	$[Zn_5Cl_4]$	2750	550 °C	18
Zn-BPZ-SA	H_2BPZ, H_2SA	$[Zn_2(Pz)_2]$	925	520 °C	This work
$Zn_3(BTP)_2$	H_3BTP	$[Zn_4(PZ)_8]$	930	510 °C	19
ZIF-8	mIM	$[ZnN_4]$	1974	500 °C	20
MIL-140C	H_2BPDC	$[ZrO(COO)_2]_n$	670	500 °C	21
MIL-53(Al)	H_2BDC	$[Al(OH)(COO)_2]_n$	1590[a]	500 °C	22
ZnBAIm	H_2BAIm	$[ZnN_4]$	701	480 °C	23
MIL-140A	H_2BDC	$[ZrO(COO)_2]_n$	415	450 °C	21
UiO-66-Br	H_2BDC-Br	$Zr_6O_4(OH)_4(COO)_{12}$	899[a]	450 °C	24
$Ni_3(BTP)_2$	H_3BTP	$[Ni_4(PZ)_8]$	1650	450 °C	19
CAU-10-H	H_2IPA	$[Al(OH)(COO)_2]_n$	627	430 °C	25
CAU-23	H_2TDC	$[Al(OH)(COO)_2]_n$	1320	430 °C	26
BUT-85	H_2PBA	$[Ni_2(OH)(H_2O)_2Pz_3]_n$	730	400 °C	27
Al-soc-MOF-1	H_4TCPT	$[V(OH)(COO)_2]_n$	5585	400 °C	28

[a]Langmuir surface area

References

[1] Krishna, R. The Maxwell-Stefan Description of Mixture Diffusion in Nanoporous Crystalline Materials. *Microporous Mesoporous Mater*. **2014**, *185*, 30-50.

[2] Krishna, R. Methodologies for Evaluation of Metal-Organic Frameworks in Separation Applications. *RSC Adv*. **2015**, *5*, 52269-52295.

[3] Krishna, R. Screening Metal-Organic Frameworks for Mixture Separations in Fixed-Bed Adsorbers using a Combined Selectivity/Capacity Metric. *RSC Adv*. **2017**, *7*, 35724-35737.

[4] Krishna, R. Methodologies for Screening and Selection of Crystalline Microporous Materials in Mixture Separations. *Sep. Purif. Techno*l. **2018**, *194*, 281-300.

[5] Krishna, R. Metrics for Evaluation and Screening of Metal-Organic Frameworks for Applications in Mixture Separations. *ACS Omega* **2020**, *5*, 16987-17004.

[6] Liu, X.; Hao, C.; Li, J.; Wang, Y.; Hou, Y.; Li, X.; Zhao, L.; Zhu, H.; Guo, W. An anionic metal-organic framework: metathesis of zinc(II) with copper(II) for efficient C_3/C_2 hydrocarbon and organic dye separation. *Inorg. Chem. Front*. **2018**, *5*, 2898-2905.

[7] Fan, W.; Wang, Y. Zhang,; Q.; Kirchon, A.; Xiao, Z.; Zhang, L.; Dai, F.; Wang, R. Sun,; D. An Amino-Functionalized Metal-Organic Framework, Based on a Rare $Ba_{12}(COO)_{18}(NO_3)_2$ Cluster, for Efficient $C_3/C_2/C_1$ Separation and Preferential Catalytic Performance. *Chem. Eur. J*. **2018**, *24*, 2137-2143.

[8] Han, X.-H.; Gong, K.; Huang, X.; Yang, J.-W.; Feng, X.; Xie, J.; Wang, B. Syntheses of Covalent Organic Frameworks via a One-Pot Suzuki Coupling and Schiff's Base Reaction for C_2H_4/C_3H_6 Separation. *Angew. Chem. Int. Ed*. **2022**, *61*, e202202912.

[9] Fan, W.; Wang, X.; Zhang, X.; Liu, X.; Wang, Y.; Kang, Z.; Dai, F.; Xu, B.; Wang, R.; Sun, D. Fine-Tuning the Pore Environment of the Microporous Cu-MOF for High Propylene Storage and Efficient Separation of Light Hydrocarbons. *ACS Cent. Sci*. **2019**, *5*, 1261-1268.

[10] Fang, H.; Zheng, B.; Zhang, Z.-H.; Li, H.-X.; Xue, D.-X.; Bai, J. Ligand-Conformer-Induced Formation of Zirconium-Organic Framework for Methane Storage and MTO Product Separation. *Angew. Chem. Int. Ed*. **2021**, *60*, 16521-16528.

[11] Chen, C.-X.; Wei, Z.-W.; Qiu, Q.-F.; Fan, Y.-Z.; Cao, C.-C.; Wang, H.-P.; Jiang, J.-J.; Fenske, D.; Su, C.-Y. A Porous Zn(II)-Metal-Organic Framework Constructed from Fluorinated Ligands for Gas Adsorption. *Cryst. Growth Des*. **2017**, *17*, 1476-1479.

[12] Geng, D.; Zhang, M.; Hang, X.; Xie, W.; Qin, Y.; Li, Q.; Bi, Y.; Zheng, Z. A 2D metal-thiacalix[4]arene porous coordination polymer with 1D channels: gas absorption/separation and frequency response. *Dalton Trans*. **2018**, *47*, 9008-9013.

[13] Zhang, Y.; Meng, X.-Q.; Ding, H.-J.; Wang, X.; Yu, M.-H.; Zhang, S.-M.; Chang, Z.; Bu, X.-H. Rational Construction of Breathing Metal-Organic Frameworks through Synergy of a Stretchy Ligand and Highly Variable π-π Interaction. *ACS Appl. Mater. Interfaces* **2019**, *11*, 20995-21003.

[14] Zheng, F.; Chen, R.; Zhang, Z.; Yang, Q.; Yang, Y.; Ren, Q.; Bao, Z. Cooperative control of intralayer and interlayer space in MOFs enables selective capture of intermediate-sized molecules. *Cell Rep. Phys. Sci*. **2022**, *3*, 100903.

[15] Wang, S.-M.; Yang, Q.-Y. A copper-based metal-organic framework for upgrading natural gas through the recovery of C_2H_6 and C_3H_8. *Green Chem. Engin.* **2023**, *4*, 81-87.

[16] Wang, C.; Zhang, J.; Wang, Z. Fluorine-Functionalized Nanoporous Polymers for Selective Adsorption/Separation of Ethylene, C_1-C_3 Alkanes, and CO_2. *ACS Appl. Nano Mater*. **2021**, *4*, 14060-14068.

[17] Cheng, H.; Wang, Q.; Meng, L.; Sheng, P.; Zhang, Z.; Ding, M.; Gao, Y.; Bai, J. Formation of a N/O/F-Rich and Rooflike Cluster-Based Highly Stable Cu(I/II)-MOF for Promising Pipeline Natural Gas Upgrading by the Recovery of Individual C_3H_8 and C_2H_6 Gases. *ACS Appl. Mater. Interfaces* **2021**, *13*, 40713-40723.

[18] Denysenko, D.; Grzywa, M.; Tonigold, M.; Streppel, B.; Krkljus, I.; Hirscher, M.; Mugnaioli, E.; Kolb, U.; Hanss, J.; Volkmer, D. Elucidating Gating Effects for Hydrogen Sorption in MFU-4-Type Triazolate-Based Metal-Organic Frameworks Featuring Different Pore Sizes. *Chem. Eur. J*. **2011**, *17*, 1837-1848.

[19] Colombo, V.; Galli, S.; Choi, H. J.; Han, G. D.; Maspero, A.; Palmisano, G.; Masciocchic, N.; Long, J. R. High thermal and chemical stability in pyrazolate-bridged metal-organic frameworks with exposed metal sites. *Chem. Sci*. **2011**, *2*, 1311-1319.

[20] Park, K. S.; Ni, Z.; A. Cote, P.; Choi, J. Y.; Huang, R.; Uribe-Romo, F. J.; Chae, H. K.; O'Keeffe, M.; Yaghi, O. M.; Exceptional chemical and thermal stability of zeolitic imidazolate frameworks. *Proc. Natl. Acad. Sci. U.S.A.* **2006**, *103*, 10186-10191.

[21] Guillerm, V.; Ragon, F.; Dan-Hardi, M.; Devic, T.; Vishnuvarthan, M.; Campo, B.; Vimont, A.; Clet, G.; Yang, Q.; Maurin, G.; Ferey, G.; Vittadini, A.; Gross, S.; Serre, C. A Series of Isoreticular, Highly Stable, Porous Zirconium Oxide Based Metal-Organic Frameworks. *Angew. Chem. Int. Ed*. **2012**, *51*, 9267-9271.

[22] Loiseau, T.; Serre, C.; Huguenard, C.; Fink, G.; Taulelle, F.; Henry, M.; Bataille, T.; Ferey, G. A Rationale for the Large Breathing of the Porous Aluminum Terephthalate (MIL-53) Upon Hydration. *Chem. Eur. J*. **2004**, *10,* 1373-1382.

[23] Luo, D.; Peng, Y.-L.; Xie, M.; Li, M.; Bezrukov, A. A.; Zuo, T.; Wang, X.-Z.; Wu, Y.; Li, Y. Y.; Lowe, A. R.; Chorążewski, M.; Grosu, Y.; Zhang, Z.; Zaworotko, M. J.; Zhou, X.-P.; Li, D. Improving Ethane/Ethylene Separation Performance under Humid Conditions by Spatially Modified Zeolitic Imidazolate Frameworks. *ACS Appl. Mater. Interfaces* **2022**, *14*, 11547-11558.

[24] Kandiah, M.; Nilsen, M. H.; Usseglio, S.; Jakobsen, S.; Olsbye, U.; Tilset, M.; Larabi, C.; Quadrelli, E. A.; Bonino, F.; Lillerud, K. P. Synthesis and Stability of Tagged UiO-66 Zr-MOFs. *Chem. Mater*. **2010**, *22*, 6632-6640.

[25] Pei, J.; Wen, H.-M.; Gu, X.-W.; Qian, Q.-L.; Yang, Y.; Cui, Y.; Li, B.; Chen, B.; Qian, G. Dense Packing of Acetylene in a Stable and Low-Cost Metal-Organic Framework for Efficient C_2H_2/CO_2 Separation. *Angew. Chem. Int. Ed*. **2021**, *60*, 25068-25074.

[26] Ye, Y.; Xian, S.; Cui, H.; Tan, K.; Gong, L.; Liang, B.; Pham, T.; Pandey, H.; Krishna, R.; Lan, P. C.; Forrest, K. A.; Space, B.; Thonhauser, T.; Li, J.; Ma, S. Metal-Organic Framework Based Hydrogen-Bonding Nanotrap for Efficient Acetylene Storage and Separation. *J. Am. Chem. Soc*. **2022**, *144*, 1681-1689.

[27] Si, G.-R.; Wu, W.; He, T.; Xu, Z.-C.; Wang, K.; Li, J.-R. Stable Bimetallic Metal-Organic Framework with Dual-Functional Pyrazolate-Carboxylate Ligand: Rational Construction and C_2H_2/CO_2 Separation. *ACS Materials Lett*. **2022**, *4*, 1032-1036.

[28] Alezi, D.; Belmabkhout, Y.; Suyetin, M.; Bhatt, P. M.; Weselinski, L. J.; Solovyeva, V.; Adil, K.; Spanopoulos, I.; Trikalitis, P. N.; Emwas, A.-H.; Eddaoudi, M. MOF Crystal Chemistry Paving the Way to Gas Storage Needs: Aluminum-Based soc-MOF for CH_4, O_2, and CO_2 Storage. *J. Am. Chem. Soc*. **2015**, *137*, 13308-13318.